JOURNAL OF COMPUTATIONAL PHYSICS **127,** 246–267 (1996)
ARTICLE NO. 0173

An Efficient Boundary Integral Method for the Mullins–Sekerka Problem

JINGYI ZHU,* XINFU CHEN,† AND THOMAS Y. HOU‡

*Department of Mathematics, University of Utah, Salt Lake City, Utah 84112; †Department of Mathematics and Statistics, University of Pittsburgh, Pittsburgh, Pennsylvania 15260; and ‡Applied Mathematics, 217-50, California Institute of Technology, Pasadena, California 91125

Received April 17, 1995; revised November 13, 1995

We use a boundary integral technique to study the two space dimensional Mullins–Sekerka free boundary problem which originates from a study of solidification and liquidation of materials of negligible specific heat. This is an area preserving and curve shortening motion. Evolution equations for the free boundaries are derived in terms of the tangent angle and total arclength, which makes a small scale decomposition possible and the Fourier transform a powerful tool in numerical calculations. With this formulation, implicit schemes can be implemented to avoid the difficult numerical stiffness associated with explicit schemes. We can compute solutions up to the time when there is a topological change, i.e., when particles touch or break up. Our numerical results for systems of a single particle or multi-particles provide some valuable information in the particle dynamics, such as the circularization of each individual particle, and the mass transfer between different particles during particle interactions.

1. INTRODUCTION

In this paper, we shall study numerically the following free boundary problem: given a bounded smooth domain Ω_0 (which may have several pieces and each piece may not be simply connected), find a continuous function $u(\mathbf{x}, t)$, $\mathbf{x} \in \mathbb{R}^2$, $t \geq 0$, and a free boundary $\Gamma = \bigcup_{t\geq 0} (\Gamma_t \times \{t\})$ such that

$$\begin{aligned} &\Delta u(\cdot, t) = 0 && \text{in } \mathbb{R}^2\backslash\Gamma_t, t \geq 0,\\ &\sup_{\mathbf{x}\in\mathbb{R}^2}|u(\mathbf{x}, t)| < \infty && \text{for all } t \geq 0,\\ &u = -\kappa && \text{on } \Gamma_t, t \geq 0,\\ &[\partial_n u]_{\Gamma_t} = -V && \text{on } \Gamma_t, t \geq 0,\\ &\Gamma_0 = \partial\Omega_0 && \text{on } \{t = 0\}, \end{aligned} \tag{1.1}$$

where κ and V are, respectively, the curvature (or the mean curvature in the high space dimensional case) and the normal velocity of Γ_t, and $[\partial_n u]_{\Gamma_t}$ is the sum of the *outward* normal derivatives of u from each side of Γ_t (which is also equal to the jump of the normal derivatives across Γ_t). Here the signs of κ and V are defined as follows. Let Ω_t be the bounded open domain such that $\partial\overline{\Omega}_t = \Gamma_t$. Then for each $\mathbf{x} \in \Gamma_t$, $V(\mathbf{x}, t)$ is positive if Γ_t moves inwards to Ω_t, and $\kappa(\mathbf{x}, t)$ is positive if the center of the osculating circle is on the side of Ω_t.

Note that (1.1) is a geometric motion problem in the sense that Γ_t depends only on the initial position Γ_0. In fact, (1.1) can be written in a short form as

$$V = [\partial_n \mathcal{K}] \tag{1.2}$$

where $\mathcal{K}$ represents the harmonic extension of the curvature κ of Γ_t over $\mathbb{R}^2$. This motion is an area preserving and curve shortening motion. To see this, let us denote by $A(t)$ the area of Ω_t and $L(t)$ the arclength of Γ_t. Then we can calculate

$$\frac{d}{dt}A(t) = -\int_{\Gamma_t} V = \int_{\Gamma_t} [\partial_n u] = \int_{\mathbb{R}^2\backslash\Gamma_t} \Delta u = 0, \tag{1.3}$$

$$\frac{d}{dt}L(t) = -\int_{\Gamma_t} \kappa V = -\int_{\Gamma_t} u\left[\frac{\partial u}{\partial n}\right] = -\int_{\mathbb{R}^2} |\nabla u|^2 \leq 0. \tag{1.4}$$

Here the first equations in (1.3) and (1.4) are geometric identities, and the remaining equations are consequences of (1.1) and the fact that (1.1b) implies $u(\mathbf{x}, t) = C(t) + O(|\mathbf{x}|^{-1})$ and $|\nabla u(\mathbf{x}, t)| = O(|\mathbf{x}|^{-2})$ as $|\mathbf{x}| \to \infty$.

The problem (1.1) is sometimes referred to as the Mullins–Sekerka problem [22] in studying solidification and liquidation of materials of negligible specific heat. In this context, u is a scaled temperature, Ω_t is the solid region and its compliment is the liquid region which is undercooled. The boundary condition $u = -\kappa$ is derived from the Gibbs–Thomson relation and amounts to the surface tension effect. In their work, Mullins and Sekerka considered the Laplacian limit of a solidification process governed by the diffusion equation. According to their work, this quasi-stationary approximation is valid under the condition

$$\left| C_\nu \frac{T_M - T_\infty}{L_\nu} \right| \ll 1, \tag{1.5}$$

0021-9991/96 $18.00

where C_ν is the specific heat per unit volume of the liquid, L_ν is the latent heart of freezing per unit volume, and T_M and T_∞ are the equilibrium temperature at a flat interface and the initial uniform temperature, respectively. Within this regime, Mullins and Sekerka studied the linear stability of a special radially symmetric solution of (1.1) in $\mathbb{R}^3$ (with a sink or source at the infinity or the origin) and showed that the spherical shape of the interface (i.e., Γ_t) is stable when the radius of the interface is small, and otherwise it is unstable.

In a different context, the problem (1.1) can be obtained as an asymptotic limit, as $\varepsilon \searrow 0$ of the Cahn–Hilliard equation $\phi_t = \Delta(-\varepsilon\Delta\phi + \varepsilon^{-1}f(\phi))$, where f is the derivative of a double equal well potential F; a typical example is $F = \frac{1}{4}(\phi^2 - 1)^2$. Mathematically, it is convenient to write the Cahn–Hilliard equation as the system

$$\begin{aligned} &\phi_t^\varepsilon(x,t) = \Delta u^\varepsilon(x,t), && (x,t) \in R^N \times (0,\infty), \\ &u^\varepsilon = -\varepsilon\Delta\phi^\varepsilon + \varepsilon^{-1}f(\phi^\varepsilon), && (x,t) \in R^N \times [0,\infty), \\ &\phi^\varepsilon(x,0) = \phi_0^\varepsilon(x), && x \in \Omega. \end{aligned} \tag{1.6}$$

Note that (1.6) differs from the usual Cahn–Hilliard equation (see [9]) only in the scaling of time, where t here corresponds to t/ε in the usual formulation. Equation (1.6) is widely accepted as a good continuum model to describe the complicated phase separation (in the original time scale) and coarsening (in our current time scale) phenomena in a melted alloy that is quenched to a temperature at which only two different concentration phases can exist in a stable way. Here u^ε is the chemical potential and ϕ^ε is a scaled concentration, where $\phi^\varepsilon = \pm 1$ represents the two stable modes. The parameter ε is the ''interaction length'' which is considered to be very small.

We now briefly describe the dynamics of the Cahn–Hilliard equation. The evolution of the concentration undergoes two stages called phase separation and phase coarsening, respectively. During the first stage, the alloy becomes a fine-grained mixture of two different phases, each of which corresponds to a stable concentration configuration. This stage usually takes a relatively short time during which the nucleation, spinodal decomposition, and formation of the phases can be observed. In terms of Eq. (1.6), the solution ϕ^ε quickly approximates the value 1 in one region $\tilde{\Omega}_t^+$ and the value -1 in another region $\tilde{\Omega}_t^-$, whereas the remaining region $\tilde{\Gamma}_t \equiv \Omega\backslash(\tilde{\Omega}_t^+ \cup \tilde{\Omega}_t^-)$ is a thin region, and it usually can be treated as an interface. At the end of the first stage, one can formally show that the energy $\mathscr{E}^\varepsilon(t) = \int_\Omega[(\varepsilon/2)|\nabla\phi^\varepsilon|^2 + (1/\varepsilon)F(\phi^\varepsilon)]$ is proportional to the total area of the interface.

When the phase regions are formed, the evolution of the concentration enters into the second stage during which the phase regions are coarsened, the originally fine-grained structure becomes less fine, and the geometric shapes of the phase regions become simpler and simpler, eventually tending to regions of minimum surface area. In terms of the Cahn–Hilliard equation (1.6), this phenomenon corresponds to the behavior of the solution that the interface moves and eventually tends to a surface having minimum surface area (whereas its enclosed region has a fixed volume).

It was formally derived by Pego [23] that, as $\varepsilon \searrow 0$, the function u^ε tends to a limit u, which, together with a free boundary $\Gamma \equiv \bigcup_{0\le t\le T}(\Gamma_t \times \{t\})$, solves the free boundary problem (1.1). Also $\phi^\varepsilon \to \pm 1$ in $\tilde{\Omega}_t^\pm$ for all $t \in [0, T]$. Rigorous justification of this formal derivation was recently carried out by Alikakos, Bates, and Chen [1] in the time interval where (1.1) has a smooth solution. More recently, Chen [10] proved that solutions of (1.6) approach a weak solution of (1.1) global in time. If we consider the free boundary problem in this context, the weak formulation of (1.1) ensures that when a particle shrinks to a single point, the extended motion is obtained by simply removing this point.

In this paper, we introduce an integral formulation of the free-boundary problem (1.1) and develop an efficient method to solve the system numerically. Concerning numerical studies of similar problems, among others, Voorhees, McFadden, Boisvert, and Meiron studied the Ostwald ripening problem [28] for the free-space with finitely many punched holes. The system they considered is different from ours in that the Laplace equation is solved only inside the region, whereas in our case the equation is solved on both sides of the interface. As a consequence, a dipole formulation is used in their work but a source formulation appears in our system, with a constraint at infinity. For this type of problem, there are two ingredients in a numerical approach: a solution to an integral equation and a scheme to evolve the free boundary. In [28], a very effective scheme to calculate the operator ∂_n was developed which transfers a boundary value to the normal derivative of its harmonic extension. Nevertheless, the time evolution of the interface in the method was treated explicitly, and the scheme requires a stability condition $\Delta t = O(h^3)$, where Δt and h are the time step and the minimal distance between two neighboring points on the curve, respectively. They also developed an effective iterative approach to solve the singular integral equation of the second kind. In our case, the difficulty of the numerical stability would remain, if we used an explicit scheme. But our integral equation has a form that is different from Fredholm equations and the kernel is derived from a source formulation. The dense matrix we obtained is similar to the matrix associated with a Fredholm integral equation of the first kind, which is known to be more difficult to deal with. However, in our system the matrix is expanded by a constraint condition and preconditioning of the matrix is possible. In the case

of a single particle we have explicitly found a quite efficient preconditioner.

To make implicit time stepping possible, we use a new formulation, developed by Hou, Lowengrub, and Shelley [18], to describe the interfacial motion. The problem we consider here is different from those considered in [18] in that we have a number of components in the region and each of the components can be multiply connected. Therefore, the interaction between the different components is extremely important and efforts should be made to couple this interaction in the motion of the particles. As the interaction is determined through the integral system mentioned above for each fixed time and the kernel involved is a source type which is different from the kernels considered in [18], it is not obvious how this should be reflected in the determination of the velocities for each particle interface. In this work, we extend the interfacial motion formulation in [18] to the multi-component case and perform a small-scale decomposition for this particular kernel. As a consequence, we obtain a system of interface motion equations for all particles in the system with enough coupling between different particles through the integral system. Further advantage is obtained by working on the Fourier space, where the singularity of the integral kernel can be handled exactly. This approach allows time steps controlled only by the CFL condition, rather than the stringent $\Delta t = O(h^3)$ restriction required in an explicit method, therefore making it realistic to calculate up to the time that some singularity forms. In our numerical calculations, we study a number of different particle configurations with up to 10 particles in the system (the number of particles we can deal with is not limited, but we use 10 particles here just to be able to pay close attention to the short-range particle dynamics). In an effort to validate the numerical scheme, first we choose the case with concentric circles where the exact solution is available, and then we derive an approximate system for two particles which can be solved exactly. Our numerical results agree extremely well with these two solutions. Next we study the circularization behavior of a single particle and two-particle interactions in several different configurations. Then we continue the process by adding more particles to the system. The interesting mass transfer dynamics between the particles is observed in all of our calculations, with a strong dependence on the configuration of the particles. Since we can add many more particles to the system, it makes this numerical tool very useful to study practical particle systems.

There are other numerical works on this free boundary problem. Recently, Bates, Chen, and Deng [6] studied numerically the very same problem. They used the same integral formulation and an implicit method to evolve the interface. However, the method is not efficient since it involves computing the inverse of a large full matrix by Guassian elimination. The advantage of that method is that it works for any piecewise smooth initial curves, so it can be very useful to study singularity formations. However, since it needs the explicit inverse of a matrix, the method can handle only about a maximum of 300 points, on a normal workstation (in about one half hour). This limits large scale calculations for a large system of particles.

On the applications of the small scale decomposition technique, recently Jou, Leo, and Lowengrub [19] used it to simulate the diffusional evolution of microstructures produced by solid-state diffusional transformations in elastically stressed binary alloys in two dimensions. The formulation also involves a log term which shares a difficulty similar to ours. They also used preconditioning GMRES iterations to accelerate the convergence of the solution to the integral system.

We also learnt that Akaiwa and Meiron [2] have worked on a similar problem using a double layer potential formulation and the $\theta - L$ formulation. They are interested in studying the statistical behavior of particle interactions with a large number of particles. The fast multipole algorithm [17] is used in obtaining efficient evaluations of the singular integrals [2].

Regarding the analysis works of this free boundary problem, Chen [11] studied the well-posedness of Problem (1.1) in the two space dimensional case. It is shown that there exists a local (in time) solution in $L^\infty(0, T; H^{5/2})$ when Γ_0 is the union of finitely many $H^{5/2}$ disjoint closed curves. Also, if Γ_0 is a single curve which is close to a circle (in $H^{5/2}$), it is shown that there exists a global solution and the solution approaches a circle at an exponential rate. Very recently, Chen, Hong, and Yi [12] established the local (in time) existence of a unique classical solution to (1.1) for arbitrary space dimensions. They proved that for any $C^{3+\alpha}$ initial data, the solution is C^∞ in $(0, T)$, where T is the maximum existence time interval of a classical solution. Global (in time) existence of weak solutions of (1.1) is recently established in [10].

The rest of the paper is organized in the following way. In Section 2, we introduce the integral formulation of the free boundary problem (1.1), and discuss the $\theta - L$ formulation for the moving interface. A small-scale decomposition for this particular integral operator is performed and the evolution equations for the tangent angles of all particles are obtained in the Fourier space, with the particle interaction effects shown explicitly. In Section 3, we describe our numerical implementation of the method. The discretization of the integral equation is discussed in detail and a preconditioner is given. In Section 4, some of the exact and approximate analytical solutions are derived so that we will be able to verify and compare our numerical results later. In Section 5, we show our numerical results for several different configurations of the particles and compare our solutions to the analytical solutions when they are available. In Section 6 we give our concluding remarks.

2. REFORMULATION OF THE PROBLEM

In our approach to the problem (1.1), there are three ingredients involved. First, we derive a boundary integral representation reformulating the problem. Then, we consider the evolution of the interface in a $\theta - L$ formulation. Consequently, the evolution equation is solved in the Fourier space, with an implicit scheme to deal with the numerical stability issue. In the last part, we solve a discretized integral system for the velocity, with the singular part handled exactly by discrete Fourier transforms.

2.1. *An Integral Characterization*

Since u in (1.1) is harmonic off Γ_t and is continuous in $\mathbb{R}^2$, we can represent u by a boundary integral involving the fundamental solution $G = (1/2\pi)\log|\mathbf{x} - \mathbf{y}|$ and the jump of the normal derivatives of u across Γ_t. The immediate advantage of this approach is that the space dimension of the problem will be reduced by one. Instead of solving the two space dimension PDE problem, we will only solve the integral equations along the boundaries of the evolving domains. This approach has been used successfully in many problems, such as water waves [3, 4], Ostwald ripening [28], Hele–Shaw flows [27, 14, 13, 18], Laplace equation in multiply connected domains [16], vortex sheet motion for inviscid fluids [21, 3, 5, 25, 18], and crystal growth [26, 24].

First we present an integral formulation which is equivalent to (1.1), or equivalently, to (1.2).

LEMMA 2.1. *Let $T > 0$ be a fixed constant. A space-time hypersurface $\Gamma = \cup_{t\in[0,T]}(\Gamma_t \times \{t\})$ is a (classical) solution to problem* (1.1) (*or* (1.2)) *if and only if there exists a function $C(t) \in C^0([0, T])$ such that*

$$-\kappa(\mathbf{x}, t) = C(t) + \frac{1}{2\pi}\int_{\Gamma_t}\log|\mathbf{x} - \mathbf{y}|V(\mathbf{y}, t)\,dS_{\mathbf{y}} \qquad \forall \mathbf{x} \in \Gamma_t, t \in [0, T],$$

$$\int_{\Gamma_t} V(\mathbf{y}, t)\,dS_{\mathbf{y}} = 0 \qquad \forall t \in [0, T]. \tag{2.1}$$

Proof. The equivalent form (2.1) was first observed and used by Chen in [11]. We sketch the proof below for reader's convenience as well as for completeness.

Assume that (u, Γ) solves (1.1). Then from (1.3), (2.1b) holds. In addition, for any $t \in [0, T]$ and $\mathbf{x} \notin \Gamma_t$,

$$0 = \frac{1}{2\pi}\iint_{\mathbb{R}^2\setminus\Gamma_t}\Delta u(\mathbf{y}, t)\log|\mathbf{x} - \mathbf{y}|\,d\mathbf{y}$$

$$= \frac{1}{2\pi}\int_{\Gamma_t}[\partial_n u]\log|\mathbf{x} - \mathbf{y}|\,dS_{\mathbf{y}} + u(\mathbf{x}, t) - u(\infty, t)$$

by Green's formula and the fact that as $|\mathbf{y}| \to \infty$, $u(\mathbf{y}, t) = u(\infty, t) + O(|\mathbf{y}|^{-1})$, and $\nabla u(\mathbf{y}, t) = O(|\mathbf{y}|^{-2})$. Setting $C(t) = u(\infty, t)$, replacing $[\partial_n u]$ by $-V$, and sending $\mathbf{x} \to \Gamma_t$, we obtain (2.1a).

Now assume that (Γ, C) satisfies (2.1). Define

$$u(\mathbf{x}, t) = C(t) + \frac{1}{2\pi}\int_{\Gamma_t}\log|\mathbf{x} - \mathbf{y}|V(\mathbf{y}, t)\,dS_{\mathbf{y}} \qquad \forall \mathbf{x} \in \mathbb{R}^2, t \in [0, T].$$

Then, by the theory of single layer potential, we know that $u(\cdot, t)$ is harmonic in $\mathbb{R}^2\setminus\Gamma_t$, and that $[\partial_n u]|_{\Gamma_t} = -V$. In addition, by (2.1a), $u = -\kappa$ on Γ_t. Finally, using (2.1b), we have, when $|\mathbf{x}| \to \infty$,

$$u(\mathbf{x}, t) = C(t) + \frac{1}{2\pi}\int_{\Gamma_t}(\log|\mathbf{x} - \mathbf{y}| - \log|\mathbf{x}|)V(\mathbf{y}, t)\,dS_{\mathbf{y}} \to C(t).$$

That is, u is uniformly bounded. Therefore, (u, Γ) is a solution to (1.1), thereby completing the proof of Lemma 2.1. ∎

With the above integral formulation, the evolution of the boundaries is quite clear. Assume that Γ_t has M pieces Γ_t^l, $l = 1, ..., M$, parameterized by $\mathbf{x}^l(\alpha, t) = (x^l(\alpha, t), y(\alpha^l, t))$, $\alpha \in [0, 2\pi]$, where the orientation of Γ_t^l coincides with α. For a given time t, we can calculate the curvature of Γ_t at any point $\mathbf{x}^l(\alpha, t)$ by

$$\kappa^l(\alpha, t) = x_s^l y_{ss}^l - x_{ss}^l y_s^l = \frac{1}{(s_\alpha^l)^3}(x_\alpha^l y_{\alpha\alpha}^l - x_{\alpha\alpha}^l y_\alpha^l),$$

where $s = s^l(\alpha, t)$ is the arclength function for Γ_t^l and $s_\alpha^l = ds^l/d\alpha = |\mathbf{x}_\alpha^l| = \sqrt{(x_\alpha^l)^2 + (y_\alpha^l)^2}$. Denote by $V^l(\alpha, t)$ the normal velocity of Γ_t at $\mathbf{x}^l(\alpha, t)$, then we can solve for the normal velocity $V^l(\alpha, t)$ from the integral system

$$\frac{1}{2\pi}\sum_{m=1}^{M}\int_0^{2\pi}\log|\mathbf{x}^l(\alpha, t) - \mathbf{x}^m(\alpha, t)|V^m(\alpha', t)\,s_\alpha^m(\alpha', t)\,d\alpha' + C(t) = -\kappa^l(\alpha, t), \qquad \alpha \in [0, 2\pi], l = 1, ..., M;$$

$$\sum_{m=1}^{M}\int_0^{2\pi} V^m(\alpha', t)\,s_\alpha^m(\alpha', t)\,d\alpha' = 0. \tag{2.2}$$

The equation of motion of Γ_t is given by

$$\mathbf{x}_t^l(\alpha, t) \cdot \mathbf{n}^l(\alpha, t) = V^l(\alpha, t), \quad \alpha \in [0, 2\pi], l = 1, ..., M \tag{2.3}$$

where $\mathbf{n}^l(\alpha, t)$ is the unit inward (to Ω_t) normal of Γ_t at $\mathbf{x}^l(\alpha, t)$:

$$\mathbf{n}^l(\alpha, t) = (-y_s^l, x_s^l) = \frac{1}{s_\alpha^l}(-y_\alpha^l(\alpha, t), x_\alpha^l(\alpha, t)),$$

$$\alpha \in [0, 2\pi], l = 1, ..., M.$$

A straightforward numerical scheme for the above evolution system can be implemented as follows. We can introduce a collection of marker points and discretize the above system. Assume that Γ_t is known in terms of these marker points. We calculate the unit normal vector $\mathbf{n}$, the arclength function s, and the curvature κ for Γ_t. Then we can solve (2.2) to obtain the normal velocity V at time t. Finally, we can use Euler's forward scheme to solve (2.3) to update $\Gamma_{t+\Delta t}$ from Γ_t, thereby completing the evolution process from time t to time $t + \Delta t$. However, there is a serious numerical stability issue in this approach. First we note that we need to calculate the unit normal vector at a marker point, based on the locations of the other markers. It is well known that this introduces a very serious numerical difficulty. For example, it will be very difficult to approximate the first and second derivatives when two neighboring points get very close. Furthermore, as shown in [28], an explicit scheme will require a very stringent stability condition $\Delta t = O(h^3)$, where h is the local minimal distance between two neighboring marker points. This requirement will make large-scale calculations almost impossible. Even in some rather simple problems, it severely hinders the calculations to the extent that, the calculation cannot continue further in time, due to the rapidly decreasing time steps.

To avoid this numerical difficulty and to find possible approaches to implement implicit schemes, we use an alternative to describe the motion of interfaces: the $\theta - L$ approach. As we show in the next section, the stability issue can be easily resolved by a direct implementation of a particularly simple implicit scheme.

2.2. *The $\theta - L$ Formulation*

In studying the evolution of a curve which depends on the curvature, it is sometimes extremely useful to represent the curve by its tangent angle θ and total arclength L, and use the evolution equations for θ and L. This is so called the $\theta - L$ formulation. Previously it was used by Kessler, Koplik, and Levine in numerical simulations of a local geometrical model of solidification [20], and by Strain in studying unstable solidification [26]. In [18], Hou, Lowengrub, and Shelley exploited this formulation and combined it with a so-called ''small scale decomposition'' reformulation, aimed to remove the stiffness attributed to the surface tension effect. They used the technique successfully to a class of fluid motions governed by surface tension, including the Hele–Shaw flow and the inertial vortex sheet flow. Here, we shall also use this approach and carry out the small-scale decomposition to deal with the Mullins–Sekerka problem.

Consider the evolution of a simply connected closed curve with known normal velocity V. Assume that the curve is represented by the position vector $\mathbf{x}(\alpha, t)$, $\alpha \in [0, 2\pi]$ at time t. Obviously $\mathbf{x}$ is 2π-periodic in α. If $s_\alpha = |\mathbf{x}_\alpha|$ is independent of α, then the curve can be reconstructed by its tangent angle θ and total arclength L. The change of variables is given by

$$x_\alpha(\alpha, t) = \frac{L(t)}{2\pi}\cos(\theta(\alpha, t)), \quad y_\alpha(\alpha, t) = \frac{L(t)}{2\pi}\sin(\theta(\alpha, t)). \tag{2.4}$$

Clearly, the curve is uniquely determined, up to a translation, by θ and L. In order to work with these new variables, we must derive the governing equations for θ and L, which are known as the $\theta - L$ formulation to be presented below.

One essential requirement in using the change of variables in (2.4) is that s_α is independent of α; namely, α is an equal arclength parameter for the curve. To enforce this condition for all $t \geq 0$, we assume that α is an equal arclength parameter for the curve at $t = 0$, and in addition to the motion in the normal direction of the curve, there is a tangential motion, given by certain tangential velocity $U(\alpha, t) = \mathbf{x}_t \cdot \mathbf{s}$, where $\mathbf{s} = (x_s, y_s)$ is the unit tangent. We note that the tangential motion only changes the parametrization of the curve; it does not affect the evolution of the curve. However, if we choose

$$U(\alpha, t) = U_0(t) + \int_0^\alpha \theta_\alpha V \, d\alpha' - \frac{\alpha}{2\pi}\int_0^{2\pi} \theta_\alpha V \, d\alpha, \tag{2.5}$$

where $U_0(t)$ is a spatial constant which we take to be zero, then the constraint that α is an equal arclength parameter will be maintained in time as long as it is satisfied at $t = 0$. That is, s_α is independent of α, so s_α is everywhere equal to its mean,

$$s_\alpha = \frac{1}{2\pi}\int_0^{2\pi} s_\alpha(\alpha, t)\, d\alpha = \frac{L(t)}{2\pi} \quad \forall \alpha \in [0, 2\pi],$$

where $L(t)$ is the total arclength at time t. In this case, the curvature has the form

$$\kappa = \frac{\theta_\alpha}{s_\alpha} = \frac{2\pi\theta_\alpha}{L}.$$

Now with the particular choice of the tangential velocity as (2.5), we can derive from the evolution equation,

$$\mathbf{x}_t = V\mathbf{n} + U\mathbf{s},$$

the equivalent $\theta - L$ *equations* (up to a translation):

$$\begin{aligned} \theta_t &= \frac{1}{s_\alpha}(V_\alpha + \theta_\alpha U), \\ L_t &= -\int_0^{2\pi} \theta_\alpha V \, d\alpha'. \end{aligned} \tag{2.6}$$

Once we know the functions θ and L, we can easily construct the curve through integrating (2.4):

$$\begin{aligned} x(\alpha, t) &= x(0, t) + \frac{L(t)}{2\pi}\int_0^\alpha \cos(\theta(\alpha', t))\, d\alpha', \\ y(\alpha, t) &= y(0, t) + \frac{L(t)}{2\pi}\int_0^\alpha \sin(\theta(\alpha', t))\, d\alpha'. \end{aligned} \tag{2.7}$$

If there is only one curve and we are only interested in the shape of the curve, then the additive constant $\mathbf{x}(0, t) = (x(0, t), y(0, t))$ is irrelevant, since it only introduces a translation. In the case that we have more than one curve in the system, the translation is certainly nontrivial. We can supplement the above evolution equations by the evolution of a reference point in each curve,

$$\mathbf{x}_t(0, t) = V(0, t)\mathbf{n}(0, t), \tag{2.8}$$

where the inward unit normal vector can be obtained through $\mathbf{n} = (-\sin\theta, \cos\theta)$.

Remark 2.1. In the two-dimensional Mullins–Sekerka problem, it is important to calculate the area of each particle accurately and to ensure that the total area of the particles involved in the system is conserved. With the $\theta - L$ formulation, it is very easy to obtain this information from the boundary integral via the divergence theorem. For a particular particle, we have its area at time t

$$A(t) = \frac{s_\alpha}{2}\int_0^{2\pi} (x(\alpha)\sin(\theta(\alpha)) - y(\alpha)\cos(\theta(\alpha)))\, d\alpha.$$

It is also straightforward to calculate the center of mass of this particle,

$$x_c(t) = \frac{s_\alpha}{2A}\int_0^{2\pi} x^2(\alpha)\sin(\theta(\alpha))\, d\alpha,$$

$$y_c(t) = -\frac{s_\alpha}{2A}\int_0^{2\pi} y^2(\alpha)\cos(\theta(\alpha))\, d\alpha.$$

These definite integrals can be calculated by either Fourier transform or direct sum with the trapezoidal rule.

2.3. *Small Scale Decomposition and Fourier Transform*

In a geometric motion formulation, V is determined by the curve Γ_t through some physical laws. The advantage of the $\theta - L$ formulation lies in the fact that, when V is expressed in terms of θ and L, the leading order differential operator in (2.6) may be linear, so an implicit numerical method can be implemented. A good example is the curvature flow where $V = \kappa$. In this case, $\kappa = \theta_\alpha/s_\alpha$ so (2.6) reads as

$$\begin{aligned} \theta_t &= \frac{4\pi^2}{L^2}\theta_{\alpha\alpha} + \frac{4\pi^2}{L^2}\theta_\alpha\left[\int_0^\alpha \theta_\alpha^2\, d\alpha' - \frac{\alpha}{2\pi}\int_0^{2\pi}\theta_\alpha^2\, d\alpha'\right], \\ L_t &= -\frac{2\pi}{L}\int_0^{2\pi}\theta_\alpha^2\, d\alpha. \end{aligned}$$

Notice that the leading order differential operators for θ is (semi)linear and parabolic, and the system is closed for (θ, L) as long as the initial configuration is supplied.

In our case, the velocity V has a global dependence on the curvature κ, and it is more complicated. Nevertheless, if we write the solution of the integral system (2.2) as $V = \mathscr{T}[\kappa] = (1/s_\alpha)\mathscr{T}[\theta_\alpha]$, then problem (1.1) can be cast as

$$\theta_t = \frac{1}{s_\alpha}\left(\frac{1}{s_\alpha}\mathscr{T}[\theta_\alpha]_\alpha + \theta_\alpha U\right),$$

where the dependence of U on V can be replaced by the dependence on $\mathscr{T}[\theta_\alpha]$. The source of stability constraints (stiffness) should come from the leading order term, and it is only important at small spatial scales. If we restrict ourselves to the small scales, the operator $\mathscr{T}$ should simplify to some linear operator. This suggests that the operator $\mathscr{T}$ could be decomposed into a linear operator, which contains the dominating high-order term, and another operator which contains the lower order terms. This idea is so-called "small scales decomposition," introduced by Hou, Lowengrub, and Shelley in [18] to solve the Hele–Shaw and inertial vortex sheet flows.

Since the integral operator in (2.2) contains a complicated singular kernel, we want to decompose it as the sum of a linear singular operator which is independent of t and the shape of the curve, and a remainder operator which is regular. To do this, for every 2π-periodic function $v(\alpha)$, we define the operator $\mathscr{M}$ by

$$\begin{aligned} \mathscr{M}[v](\alpha) &= \frac{1}{2\pi}\int_0^{2\pi} \log|e^{i\alpha} - e^{i\alpha'}| v(\alpha')\, d\alpha' \\ &= \frac{1}{2\pi}\int_0^{2\pi} \log\left|2\sin\frac{\alpha - \alpha'}{2}\right| v(\alpha')\, d\alpha', \end{aligned} \tag{2.9}$$

and operators $\mathscr{R}^{l,m}$, $l, m = 1, ..., M$, by

$$\mathscr{R}^{l,m}[v](\alpha) = \begin{cases} \dfrac{1}{2\pi}\displaystyle\int_0^{2\pi} \log \left| \frac{\mathbf{x}^l(\alpha,t) - \mathbf{x}^l(\alpha',t)}{2\sin\left(\dfrac{\alpha-\alpha'}{2}\right)} \right| v(\alpha')\, d\alpha', & \text{if } l = m, \\ \dfrac{1}{2\pi}\displaystyle\int_0^{2\pi} \log |\mathbf{x}^l(\alpha,t) - \mathbf{x}^m(\alpha',t)|\, v(\alpha')\, d\alpha', & \text{if } l \neq m. \end{cases} \tag{2.10}$$

Then, the first equation in (2.2) can be written as

$$s_\alpha^l \mathscr{M}[V^l] + \sum_{m=1}^{M} s_\alpha^m \mathscr{R}^{l,m}[V^m] = -\frac{\theta_\alpha^l}{s_\alpha^l} - C, \quad l = 1, ..., M. \tag{2.11}$$

One can directly verify that for any periodic function v, the mean of $\mathscr{M}[v]$ is zero and that zero is a (simple) eigenvalue of $\mathscr{M}$ with the eigenfunction being the constant function. In addition,

$$D_\alpha \mathscr{M}[v](\alpha) = \frac{1}{4\pi}\int_0^{2\pi} \cot\frac{\alpha-\alpha'}{2} v(\alpha')\, d\alpha' = \frac{1}{2}\mathscr{H}[v](\alpha), \tag{2.12}$$

where $\mathscr{H}$ is the Hilbert operator on 2π-periodic functions. Recall that for every 2π-periodic function v with zero mean, $\mathscr{H}^2[v] = -v$. We then deduce from (2.12) that, for every 2π periodic function f with zero mean,

$$\mathscr{M}^{-1}[f] = c - 2\mathscr{H}[f_\alpha],$$

where c is an arbitrary constant. Thus, taking $\mathscr{M}^{-1}$ of (2.11), we have

$$V^l - \overline{V}^l = \frac{2}{(s_\alpha^l)^2}\mathscr{H}[\theta_{\alpha\alpha}^l] + \frac{2}{s_\alpha^l}\mathscr{H}\left[\sum_{m=1}^{M} s_\alpha^m \mathscr{R}^{l,m}[V^m]\right]_\alpha,$$

where $\overline{V}^l$ is the mean of V^l. Substituting this equation into (2.6), we then obtain

$$\theta_t^l = \frac{2}{(s_\alpha^l)^3}\mathscr{H}[\theta_{\alpha\alpha\alpha}^l] + \frac{2}{(s_\alpha^l)^2}\mathscr{H}\left[\sum_{m=1}^{M} s_\alpha^m \mathscr{R}^{l,m}[V^m]\right]_{\alpha\alpha} + \frac{1}{s_\alpha^l}\theta_\alpha^l U^l. \tag{2.13}$$

Clearly, the leading order operator is linear. This suggests a natural implementation of a fast implicit numerical scheme.

Since we are dealing with closed curves, it is natural to work in the Fourier space. Furthermore, differential operators and the Hilbert operator $\mathscr{H}$ have particularly simple kernels under the Fourier transformation. However, we note that θ^l is not a periodic function of α. It is incremented by a value of $2\nu^l\pi$ every time α is incremented by 2π, where ν^l is 1 if Γ^l is counterclockwisely orientated and -1 otherwise. Nevertheless, if we write

$$\theta^l(\alpha,t) = \nu^l\alpha + \phi^l(\alpha,t), \quad \alpha \in [0, 2\pi], \quad l = 1, ..., M, \tag{2.14}$$

then ϕ^l is 2π-periodic. It is therefore convenient to work with the evolution of ϕ^l, rather than that of θ^l.

For every 2π-periodic function f, we denote its Fourier transform by

$$\hat{f} = \hat{f}(k) = \frac{1}{2\pi}\int_0^{2\pi} f(\alpha')e^{-ik\alpha'}\, d\alpha',$$

for every integer k. Since for every periodic function v, $\widehat{\mathscr{H}[v]} = -i\,\mathrm{sgn}(k)\hat{v}$, where $\mathrm{sgn}(k)$ is the signature function. Substituting (2.14) into (2.13) and taking the Fourier transform on both sides of (2.13), we then obtain

$$\hat{\phi}_t^l = -\frac{2|k|^3}{(s_\alpha^l)^3}\hat{\phi}^l + \frac{2ik|k|}{(s_\alpha^l)^2}\sum_{m=1}^{M} s_\alpha^m \widehat{\mathscr{R}^{l,m}(V^m)} + \frac{1}{s_\alpha^l}\hat{g}^l \quad \forall k \tag{2.15}$$

where $g^l = U^l(\nu^l + \phi_\alpha^l)$. Clearly, the highest order corresponds to the first term on the right-hand side and it is linear in $\hat{\phi}^l$. Therefore, it provides a straightforward application of the Crank–Nicholson time discretization, to be explained in the next section.

Remark 2.2. In their paper [15], Duchon and Robert actually derived an analogous version of Eq. (2.13). In their case, $M = 1$, $\alpha \in \mathbb{R}^1$ is the arclength parameter (so that $s_\alpha = 1$), $\mathscr{H}$ is the Hilbert operator on $L^2(\mathbb{R}^1)$ functions (which has the properties $\mathscr{H}^2 = -I$ and $D_\alpha\mathscr{H} = \mathscr{H}D_\alpha$). Replacing the V dependence in (2.13) by $\mathscr{T}[\theta_\alpha]$, they used the version

$$\theta_t = \mathscr{H}[\theta_{\alpha\alpha\alpha}] + \mathscr{R}[\theta, \Gamma_t],$$

where $\mathscr{R}$ is a nonlinear "regular" operator. Here the missing factor 2 in front of $\mathscr{H}$ is due to the fact that they are dealing with the one-phase Hele–Shaw problem. With this formula, the Fourier transform, semigroup theory, and a detailed regularity analysis for the operator $\mathscr{R}$, they established the existence and uniqueness of solutions for certain initial configuration Γ_0 explained in our introduction. Since in their case, $\alpha \in (-\infty, \infty)$, the L equation in (2.6) is not needed.

3. NUMERICAL IMPLEMENTATION

3.1. *Advance of the Interface*

Since α^l is an equal arclength parameter for each curve, we can divide the curve into N^l subsections with equal arclength by taking discretization points at $\mathbf{x}^l(\alpha_j^l, t)$ with $\alpha_j^l = 2j\pi/N^l$, $j = 1, ..., N^l$.

Let Δt be the time step and let $t^n = n\Delta t$ be the time. We shall use the superscript n to denote the value of various functions at time t^n. Equation (2.15) can be discretized for all $k = 0, \pm 1, ..., \pm N^l/2$ and $l = 1, ..., M$, by a Crank–Nicholson scheme,

$$\frac{\hat{\phi}^{l,n+1} - \hat{\phi}^{l,n-1}}{2\Delta t} + \left(\frac{|k|}{s_\alpha^{l,n}}\right)^3 (\hat{\phi}^{l,n+1} + \hat{\phi}^{l,n-1}) = \hat{f}^{l,n},$$

where

$$\hat{f}^{l,n} = \frac{2ik|k|}{(s_\alpha^l)^2} \sum_{m=1}^{M} s_\alpha^{m} \widehat{\mathscr{R}^{l,m,n}(V^{m,n})} + \frac{1}{s_\alpha^l} \hat{g}^{l,n}.$$

Given the solutions $\hat{\phi}^n$, $\hat{\phi}^{n-1}$, all the information of Γ_t at $t = t^n$, as well as V^n, we can solve for $\hat{\phi}^{l,n+1}$ directly in the above system. Then we use the inverse FFT to find $\phi^{l,n+1}$. To obtain the update for $s_\alpha^{l,n+1}$ through the total arclength, we solve the L equation in (2.6) with a second-order Adams–Bashforth scheme

$$L^{l,n+1} = L^{l,n} + \frac{\Delta t}{2}(3\Psi^{l,n} - \Psi^{l,n-1}),$$

where superscripts denote the curve and the time level, and Ψ^l is given by

$$\Psi^l = -\int_0^{2\pi} (\nu^l + \phi_\alpha^l) V^l d\alpha'.$$

To reconstruct the interface at t^{n+1} from θ^{n+1} and L^{n+1}, we need to update the reference point for each curve. First we integrate (2.8):

$$x^{l,n+1}(0) = x^{l,n-1}(0) - 2V^{l,n}(0)\Delta t \sin(\phi^{l,n}(0)), \quad (3.1)$$

$$y^{l,n+1}(0) = y^{l,n-1}(0) + 2V^{l,n}(0)\Delta t \cos(\phi^{l,n}(0)). \quad (3.2)$$

Then we can obtain the inverse mapping from (θ, L) to (x, y) by integrating (2.7):

$$x^{l,n+1}(\alpha) = x^{l,n+1}(0) + \frac{L^{l,n+1}}{2\pi} \int_0^\alpha \cos(\nu^l \alpha' + \phi^{l,n+1}(\alpha'))\, d\alpha',$$

$$y^{l,n+1}(\alpha) = y^{l,n+1}(0) + \frac{L^{l,n+1}}{2\pi} \int_0^\alpha \sin(\nu^l \alpha' + \phi^{l,n+1}(\alpha'))\, d\alpha'.$$

As pointed out in [18], it is important for (x, y) to be an exact periodic function. Any numerical error may grow in time and leads to serious distortion of the closed curve. This numerical difficulty can be overcome by a correction term in the integration, such as

$$\mathbf{x}_j = \mathbf{x}_j' - \frac{j}{N}(\mathbf{x}_N' - \mathbf{x}_0), \quad j = 1, 2, ..., N,$$

where $\mathbf{x}_j'$, $j = 1, ..., N$, are the coordinates generated by the numerical quadrature and $(\mathbf{x}_N' - \mathbf{x}_0)$ represents the numerical error it causes. After applying this correction, $\mathbf{x}_N = \mathbf{x}_0$ and the curve is completely closed.

Even though our ϕ evolution is solved implicitly, the reference point for each curve is updated explicitly in (3.1) and (3.2). A CFL condition would be required. Here we use

$$\Delta t \le c \max_l \left\{ \frac{2\pi s_\alpha^l}{\max_j |v_j^l| N^l} \right\}, \quad (3.3)$$

where $c \in (0, 1]$ is a constant. At $t = 0$, we require that each curve have an equal arclength parametrization. For most closed curves, this parameter is not naturally given. We use a numerical procedure developed by Baker and Shelley [5] to reparametrize each of the initial curves.

We remark that fast Fourier transforms are used to calculate all the derivatives and integrals in the space variable, so we achieve spectral accuracy in these steps. Another advantage of using FFT is that we can double or halve the number of points on one curve very easily. This is very useful in complex dynamical problems, where the resolution requires more points on one curve and less points on another curve, at different times. To double the number of points on one curve we just need to change N to $2N$, extend the array for $\hat{\phi}$, and fill these high-frequency modes by zeros. The evolution equations will pick up the changes in these modes, and the inverse mapping will be taken care of automatically. A similar procedure can be used to chop off high frequency modes, if we want to halve the number of points on the curve.

Notice that so far, in the above updating procedure, the velocity V^n is assumed to be known to provide ϕ^{n+1} and Γ^{n+1}. In the next time step, we need to determine the velocity from the updated curves Γ^{n+1} through solving the integral system (2.2). It is expected that this is the most time-consuming step in the calculations. In the next subsection, we shall discuss our numerical implementation to solve (2.2), for any given curve, thereby completing the updating process.

3.2. *Solution of the Integral System*

We now consider the integral system (2.2) at a fixed time t and assume that Γ_t is known. Here we shall suppress

the time dependence in the expressions. Using the notation in Section 2.3, this system can be written as

$$s_\alpha^l \mathscr{M}[V^l] + \sum_{m=1}^M s_\alpha^m \mathscr{R}^{l,m}[V^m] + C = -k^l, \quad l = 1, ..., M,$$
$$\sum_{m=1}^M \int_0^{2\pi} s_\alpha^m V^m \, d\alpha = 0. \tag{3.4}$$

In this integral system, the terms $\mathscr{R}^{l,m}$ for $l \neq m$ represent the interaction between the lth and mth particles.

As mentioned in the previous subsection, for each curve Γ^l, $l = 1, ..., M$, we have N^l equally spaced points along the curve, given by the parameter $\alpha_j^l = 2j\pi/N^l$, $j = 1, ..., N^l$. Denote $\mathbf{x}_j^l = \mathbf{x}^l(\alpha_j)$, $v_j^l = (s_\alpha^l/N^l)\, V^l(\alpha_j)$, and $\kappa_j^l = \kappa^l(\alpha_j)$; we want to discretize the above integral system into a linear system in terms of these variables. The scaling s_α^l/N^l for v is chosen so that the resulting linear system is symmetric. Then we shall solve v_j^l in the linear system, with given κ_j^l and $\mathbf{x}_j^l$ data.

It is straightforward to discretize the regular kernels $\mathscr{R}^{l,m}$, defined in (2.10), as long as different curves are well separated. Since the singular kernel $\mathscr{M}$, defined in (2.9), has the property $D_\alpha \mathscr{M} = \frac{1}{2}\mathscr{H}$, the evaluation of this part can be efficiently and accurately carried out by using FFT. After some scaling, the resulting positive definite system to be solved is

$$\begin{pmatrix} N^1\mathscr{M}^1 + R^{1,1} & R^{1,2} & \cdots & R^{1,M} & \mathbf{p}^1 \\ R^{2,1} & N^2\mathscr{M}^2 + R^2 & \cdots & R^{2,M} & \mathbf{p}^2 \\ \vdots & \vdots & \ddots & \vdots & \vdots \\ R^{M,1} & R^{M,2} & \cdots & N^M\mathscr{M}^M + R^M & \mathbf{p}^M \\ \mathbf{p}^{1,T} & \mathbf{p}^{2,T} & \cdots & \mathbf{p}^{M,T} & 0 \end{pmatrix} \begin{pmatrix} \mathbf{v}^1 \\ \mathbf{v}^2 \\ \vdots \\ \mathbf{v}^M \\ C \end{pmatrix} = - \begin{pmatrix} \kappa^1 \\ \kappa^2 \\ \vdots \\ \kappa^M \\ 0 \end{pmatrix} \tag{3.5}$$

Here the matrices $R^{l,m}$ are given by

$$R_{i,j}^{l,m} = \begin{cases} \log \left| \dfrac{\mathbf{x}_i^l - \mathbf{x}_j^l}{2\sin((\pi/N^l)(i-j))} \right|, & i \neq j, l = m, \\ \log s_\alpha^l, & i = j, l = m, \\ \log|\mathbf{x}_i^l - \mathbf{x}_j^m|, & l \neq m. \end{cases}$$

The N^l-dimensional vectors $\mathbf{p}^l$, $\mathbf{v}^l$, and κ^l are given by

$$\mathbf{p}^l = (1, 1, ..., 1)^{\mathrm{T}},$$
$$\mathbf{v}^l = (v_1^l, v_2^l, ..., v_{N^l}^l)^{\mathrm{T}},$$
$$\kappa^l = (\kappa_1^l, \kappa_2^l, ..., \kappa_{N^l}^l)^{\mathrm{T}}.$$

As we note, the resulting matrix is symmetric, but it has a full structure, as opposed to the usually sparse matrices arising from elliptic PDEs. However, this does not imply that we cannot use standard iterative methods to solve the full linear system. In this time-dependent problem, iterative methods are particularly attractive as we have very good initial guesses from the solution at the previous time step. In this work, since the matrix in (3.5) is positive definite, we use the standard conjugate gradient method to solve the linear system.

3.3. *Preconditioner for One-Particle Systems*

Conjugate gradient method usually works best when some good preconditioners are available. In the cases where particles are well separated, the inter-particle interactions are rather weak, so that the unpreconditioned conjugate gradient method gives acceptable performance. Nevertheless, a good preconditioner would be valuable when we deal with large systems where some particles may become very close with each other. For particles separated by a large distance, the point source approximation can be a good candidate. In the case where some particles are very close to each other, the search for a good preconditioner can be very difficult.

In the case that there is only one particle in the system, we have found a rather powerful preconditioner for the linear system (3.5). The linear system in this case is

$$\begin{pmatrix} N\mathscr{M} + R & \mathbf{p} \\ \mathbf{p}^{\mathrm{T}} & 0 \end{pmatrix} \cdot \begin{pmatrix} \mathbf{v} \\ C \end{pmatrix} = \begin{pmatrix} -\kappa \\ 0 \end{pmatrix},$$

where $\mathbf{p} = (1, 1, 1, ..., 1)^{\mathrm{T}}$, $\mathbf{v} = (s_\alpha/N)\,(V_1, V_2, ..., V_N)^{\mathrm{T}}$, and $\kappa = (\kappa_1, \kappa_2, ..., \kappa_N)^{\mathrm{T}}$.

The preconditioner we use here is

$$M'\mathbf{z} = \begin{pmatrix} N\mathscr{M} & \mathbf{p} \\ \mathbf{p}^{\mathrm{T}} & 0 \end{pmatrix} \cdot \begin{pmatrix} \mathbf{z}' \\ z_{N+1} \end{pmatrix} = \mathbf{r} = \begin{pmatrix} \mathbf{r}' \\ r_{N+1} \end{pmatrix},$$

or

$$N\mathscr{M}\mathbf{z}' + z_{N+1}\mathbf{p} = \mathbf{r}', \qquad \sum_{i=1}^N z_i = r_{N+1}. \tag{3.6}$$

Since $\mathscr{M}\mathbf{p} = 0$, $\mathscr{M}$ is symmetric, and the rank of $\mathscr{M}$ is $N - 1$, the solvability condition for (3.6) gives

$$z_{N+1} = \frac{1}{N}\sum_{i=1}^{N} r_i$$

and $\mathbf{z}'$ is given by

$$\mathbf{z}' = \mathscr{M}^{-1}(\mathbf{r}' - z_{N+1}\mathbf{p}).$$

The inverse of $\mathscr{M}$ can be easily performed by using FFT.

This preconditioner is motivated by a direct physical consideration. The integral kernel is dominated by the interval near the point $\mathbf{x}(\alpha)$, where it can be approximated by a circle, if the curve is locally smooth. The matrix R represents the deviation of the curve from the circle. If we ignore the deviation, we are dealing with a circle, which can be inverted exactly in the Fourier space. The solvability condition checks the curvature distribution, since the normal velocity distribution along the curve is determined by the distribution of the curvature. Therefore, we need to translate the curvature distribution so the right-hand side for $\mathscr{M}\mathbf{z}$ has zero mean.

4. SOME EXACT AND APPROXIMATE SOLUTIONS

In this section, we derive some special solutions to be used to verify our numerical solutions. First, we find a special solution to the original free-boundary problem in the concentric circle case. Then we derive a simplified system which approximates the interaction of two initially circular particles separated by a large distance. The simplified system leads to an ODE system, which can be easily solved numerically.

4.1. *Concentric Circles*

Assume that we have M concentric circles: C_i, $i = 1, ..., M$, with radii R_i satisfying $R_1 < R_2 < \cdots < R_M$. Taking clockwise orientation for the smallest circle, we then have $\kappa = (-1)^i R_i^{-1}$, on C_i, $i = 1, ..., M$. Hence, denote $\kappa_i = (-1)^i R_i^{-1}$ for $i = 1, ..., M$, $\kappa_0 = \kappa_1$, $\kappa_{M+1} = \kappa_M$, $R_0 = 0$, and $R_{M+1} = \infty$, we have that

$$u(r, t) = \kappa_{i-1} + \frac{\log r - \log R_{i-1}}{\log R_i - \log R_{i-1}}(\kappa_i - \kappa_{i-1})$$

for all $r \in [R_{i-1}, R_i]$, $i = 1, ..., M + 1$. Consequently, the sum of the outward normal derivatives at $r = R_i$ is

$$[\partial_n u]|_{C_i} = \frac{1}{R_i}\frac{\kappa_i - \kappa_{i-1}}{\log R_i - \log R_{i-1}} - \frac{1}{R_i}\frac{\kappa_{i+1} - \kappa_i}{\log R_{i+1} - \log R_i}$$

$$= \frac{(-1)^i}{R_i}\left[\frac{1/R_i + 1/(R_{i-1})}{\log R_i - \log R_{i-1}} + \frac{1/R_{i+1} + 1/R_i}{\log R_{i+1} - \log R_i}\right].$$

From the equation $V|_{C_i} = (-1)^i \dot{R}_i$ and $V = -[\partial_n u]$; we then obtain the governing equations for the motion of concentric circles,

$$\frac{d}{dt}R_i = -\frac{1}{R_i}[f_i(\mathbf{R}) + f_{i+1}(\mathbf{R})], \quad i = 1, ..., M,$$

where

$$f_i(\mathbf{R}) = \begin{cases} \dfrac{R_i^{-1} + R_{i-1}^{-1}}{\log R_i - \log R_{i-1}}, & i = 2, ..., M, \\ 0, & i = 1, M + 1. \end{cases}$$

The Case of Two Circles. In this case, we have that

$$\frac{d}{dt}R_1^2 = \frac{d}{dt}R_2^2 = -\frac{2(R_1^{-1} + R_2^{-1})}{\log R_2 - \log R_1}.$$

Assume that $R_1(0) = r_1$ and $A^2 = R_2^2(0) - R_1^2(0)$. Then we have

$$R_2(t) = \sqrt{A^2 + R_1^2(t)},$$

so that

$$\begin{aligned} t &= -\frac{1}{2}\int_{R_1}^{r_1} \frac{r^2\sqrt{r^2 + A^2}\log(1 + A^2/r^2)}{r + \sqrt{r^2 + A^2}}\,dr \\ &= A^3\int_{r_1/A}^{R_1/A} \frac{s^2\sqrt{1 + s^2}\,[\log\sqrt{1 + s^2} - \log s]}{s + \sqrt{1 + s^2}}\,ds. \end{aligned} \tag{4.1}$$

This defines a function $R_1(t)$ implicitly for $t \in [0, T]$, where T is the time that the inner circle is reduced to a point. Numerically, we can use any quadrature rule to plot this function.

4.2. *Exact Solution for a Modified System*

Since it is very difficult to obtain exact solutions, for the purpose of comparing with our numerical results we shall now provide another example where exact solutions are obtained for a system which is modified from the original system by making a known correction to the normal velocity. As shall be seen below, this example will provide some insight on the original system we study in this paper.

Consider the system which starts with two disjoint circles. If the size of these two circles are the same, they are in an equilibrium state; otherwise, they will evolve. Formal argument and numerical experiments show that the smaller

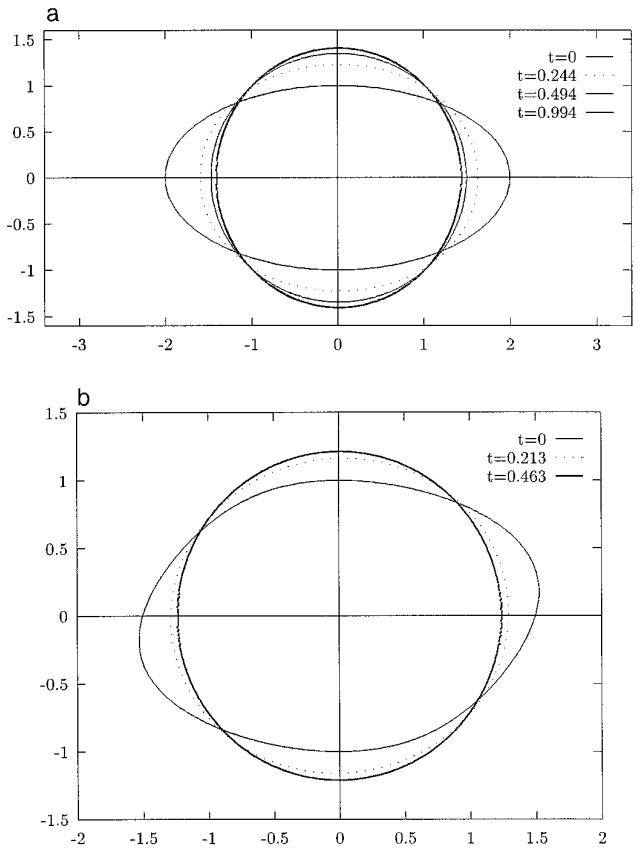

FIG. 1. Examples of single particle circularizing: (a) an elliptic particle, $N = 256$; (b) a perturbed elliptic particle, $N = 512$.

one will shrink and disappear in a finite time, whereas the larger one becomes larger and larger, until it "eats up" the smaller one in a "remote" way. If the initial distance between two circles is large, formal argument shows that each particle will stay very close to a circular shape, while their (geometric) centers and sizes change quite appreciably.

Based on this observation, in the following, we shall construct an exact solution to a *velocity corrected system*

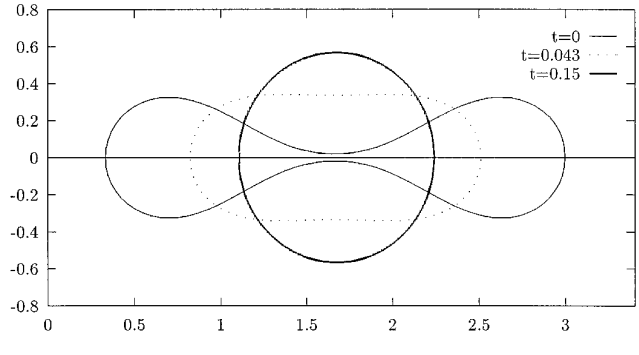

FIG. 2. A dumbbell shaped particle, $N = 128$.

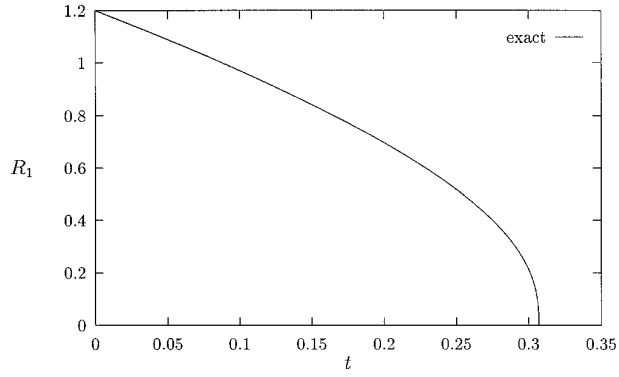

FIG. 3. The inner radius R_1 of the concentric circular region, as a function of t, calculated from solving the full free-boundary system and from solving the ODE problem.

such that only the essential motion of the center and the size of the circles are captured, whereas the change of the particle shape is ignored.

Now assume that the two circles C_i are centered at z_i with radius R_i, $i = 1, 2$. Here we assume that z_1, z_2 are real, $R_2 > R_1$ and $z_1 - z_2 > R_1 + R_2$. Set

$$d = z_1 - z_2,$$

$$\overline{z} = \frac{(z_1 - z_2)}{2},$$

$$b = \overline{z} + \frac{R_1^2 - R_2^2}{2d},$$

$$a = \frac{d}{2}\sqrt{\left[1 - \left(\frac{R_1 + R_2}{d}\right)^2\right]\left[1 - \left(\frac{R_1 - R_2}{d}\right)^2\right]}.$$

Then one can easily verify that

$$z_1 = b + \sqrt{a^2 + R_1^2}, \quad z_2 = b - \sqrt{a^2 + R_2^2}.$$

Consider the analytic function

$$U(z) = \frac{1}{R_1} + A\left\{\log\frac{z - b + a}{z - b - a} - \log(\sqrt{a^2 + R_1^2} + a) + \log R_1\right\},$$

where $z = x + iy$ and

$$A = \frac{R_1^{-1} - R_2^{-1}}{\log(\sqrt{a^2 + R_1^2} + a) - \log R_1 + \log(\sqrt{a^2 + R_2^2} + a) - \log R_2}.$$

Since on C_i,

$$\left|\frac{z - b + a}{z - b - a}\right| = \sqrt{1 + a^2/R_i^2} + (-1)^{i+1}\frac{a}{R_i} = \frac{R_i}{\sqrt{a^2 + R_i^2} + (-1)^i a},$$

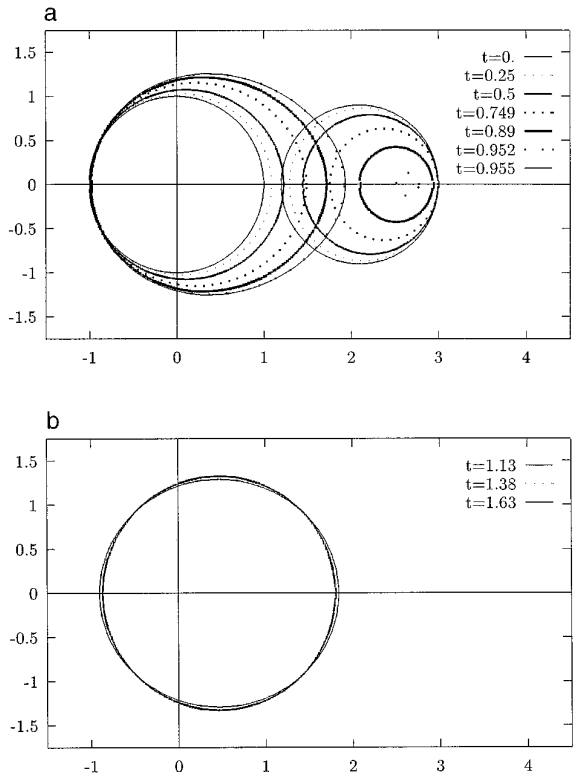

FIG. 4. Two initially circular particles with different radii, with mass transfer from the smaller particle to the larger particle, $N = 256$: (a) early time before the smaller particle disappears; (b) the circularizing of the surviving particle.

one can directly verify that the real part of $U(z)$ on C_i is $1/R_i$. Hence, the function $u(x, y)$ defined by

$$u(x,y) = \begin{cases} R_i^{-1} & \text{inside of } C_i,\ i = 1, 2, \\ \mathrm{Re}(U(x+iy)) & \text{otherwise,} \end{cases}$$

is harmonic off C_i and equal to the curvature of C_i on C_i.

Notice that

$$u_x - iu_y = U_z = A\left[\frac{1}{z-b+a} - \frac{1}{z-b-a}\right]$$

outside of C_1 and C_2. It follows that, on C_i, writing, $z = z_i + R_i e^{i\theta}$,

$$u_x - iu_y = A\left[\frac{1}{R_i e^{i\theta} + (-1)^{i+1}\sqrt{a^2+R_i^2}+a} - \frac{1}{R_i e^{i\theta} + (-1)^{i+1}\sqrt{a^2+R_i^2}-a}\right]$$

$$= -\frac{aAe^{-i\theta}}{R_i^2}\frac{1}{\cos\theta + (-1)^{i+1}\sqrt{1+a^2/R_i^2}}.$$

Hence, on C_i,

$$\begin{aligned}[u_n] &= \left[\frac{\partial u}{\partial n}\right]\Bigg|_{z=z_i+R_i e^{i\theta}} \\ &= \frac{aA}{R_i^2(\cos\theta + (-1)^{i+1}\sqrt{1+a^2/R_i^2})} \\ &= \frac{(-1)^i A}{R_i}\left\{1 + 2\sum_{n=1}^{\infty}\left[\frac{(-1)^i R_i}{\sqrt{a^2+R_i^2}+a}\right]^n \cos(n\theta)\right\}.\end{aligned} \tag{4.2}$$

Now consider the motion such that the normal velocity V is taken only for the first three modes of the Fourier transformation of $[u_n]$ in (4.2); namely,

$$\begin{aligned}V(z(\theta,t)) = {}& \tfrac{1}{2}\langle[u_n], 1\rangle + \langle[u_n], \cos\theta\rangle\cos\theta \\ &+ \langle[u_n], \sin\theta\rangle\sin\theta,\end{aligned} \tag{4.3}$$

where $\langle f, g\rangle = 1/\pi \int_0^{2\pi} fg\, d\theta$.

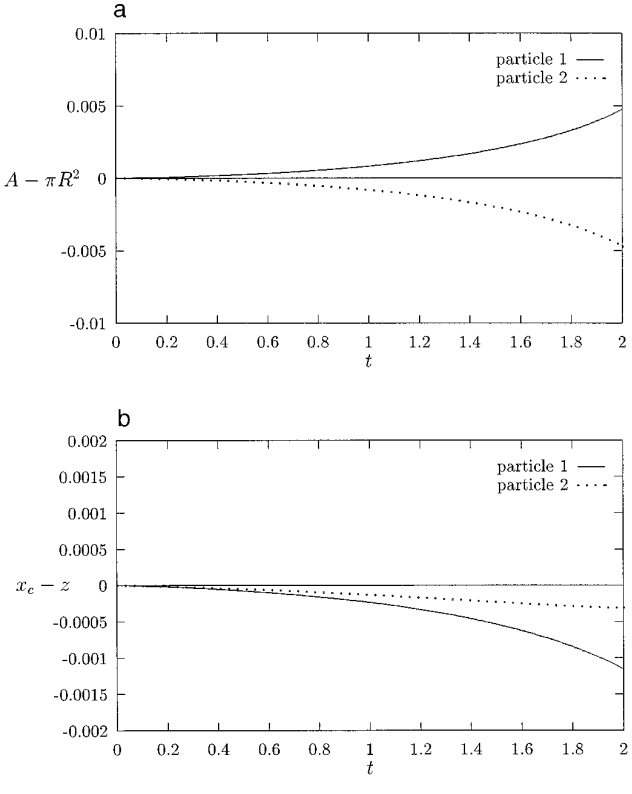

FIG. 5. Comparisons of the full equation solutions to the modified ODE solutions in the case of two initially circular particles: (a) the comparison of areas; (b) the comparison of centers of mass.

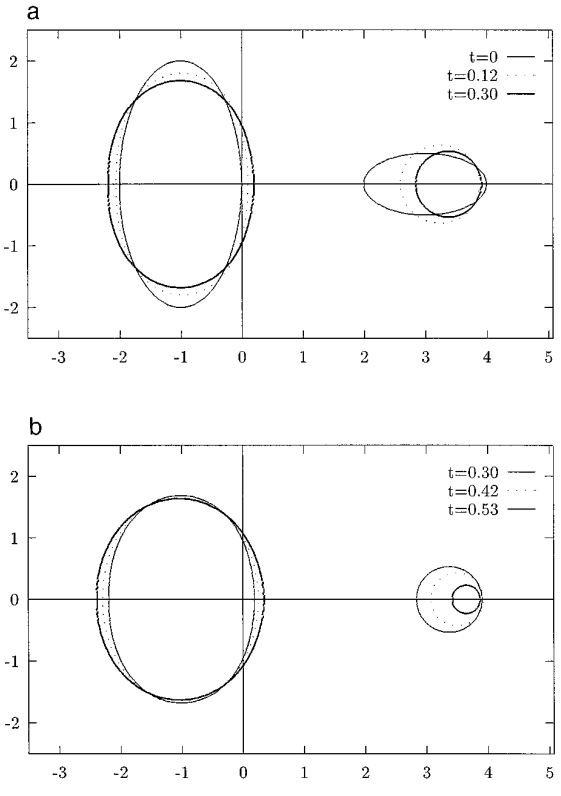

FIG. 6. Two initially elliptic particles at different times, $N = 384$.

Denoting the circles at time t by

$$z^i(\theta, t) = z_i(t) + R_i(t)e^{i\theta}, \quad i = 1, 2, \tag{4.4}$$

we have that

$$V = \mathrm{Re}(z_t^i e^{-i\theta}) = z_i'(t)\cos\theta + R_i'(t).$$

Hence, the motion of the circles represented by (4.4) is governed by (4.3), if and only if $z_i(t)$ and $R_i(t)$ satisfy the following system of ODEs,

$$\begin{aligned} R_1'(t) &= -A/R_1, \\ R_2'(t) &= A/R_2, \\ z_1'(t) &= 2A/(\sqrt{a^2 + R_1^2} + a), \\ z_2'(t) &= 2A/(\sqrt{a^2 + R_2^2} + a), \end{aligned} \tag{4.5}$$

where

$$\begin{aligned} d &= z_1 - z_2, \\ a &= \frac{d}{2}\sqrt{\left(1 - \left(\frac{R_1 + R_2}{d}\right)^2\right)\left(1 - \left(\frac{R_1 - R_2}{d}\right)^2\right)}, \end{aligned} \tag{4.6}$$

$$A = \frac{R_2 - R_1}{R_1 R_2\,[\log(\sqrt{a^2 + R_1^2} + a) + \log(\sqrt{a^2 + R_2^2} + a) - \log(R_1 R_2)]}.$$

LEMMA 4.1. *Given* $R_1(0)$, $R_2(0)$, $z_1(0)$, $z_2(0)$ *satisfying* $R_2(0) > R_1(0)$, $z_1(0) - z_2(0) > R_1(0) + R_2(0)$, *there exists a finite time* $T > 0$ *such that the ODE system* (4.5) *with a, d, A defined in* (4.6) *has a unique solution in* $[0, T)$, *and at time* T, $R_1 = 0$. *In addition, in* $[0, T)$,

$$\begin{aligned} &R_1' > 0, \quad R_2' < 0, \quad z_1' > 0, \quad z_2' > 0, \quad (R_1 + z_1)' < 0, \\ &(z_1 - R_1)' > 0, \quad (z_2 - R_2)' < 0, \quad (z_2 + R_2)' > 0. \end{aligned}$$

That is, the motion has the following properties:

1. *the centers of two circles move to the right* (*the direction of smaller circle*);
2. *the larger circle becomes larger*, *the smaller one becomes smaller, and the total area of the two circles is preserved*;

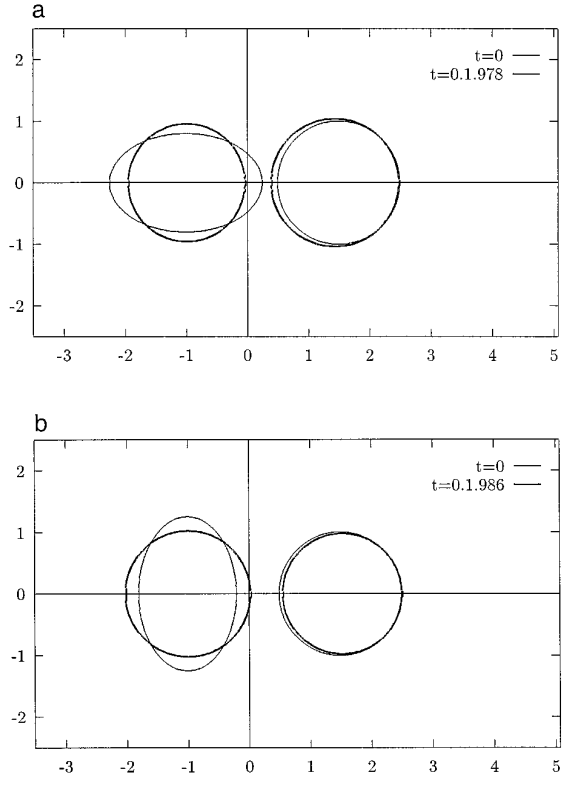

FIG. 7. Two particles with the same initial mass (area), but different shapes, $N = 256$: (a) the major axis of the initial ellipse is aligned with the x-axis; (b) the major axis of the initial ellipse has an angle of $\pi/2$ with the x-axis.

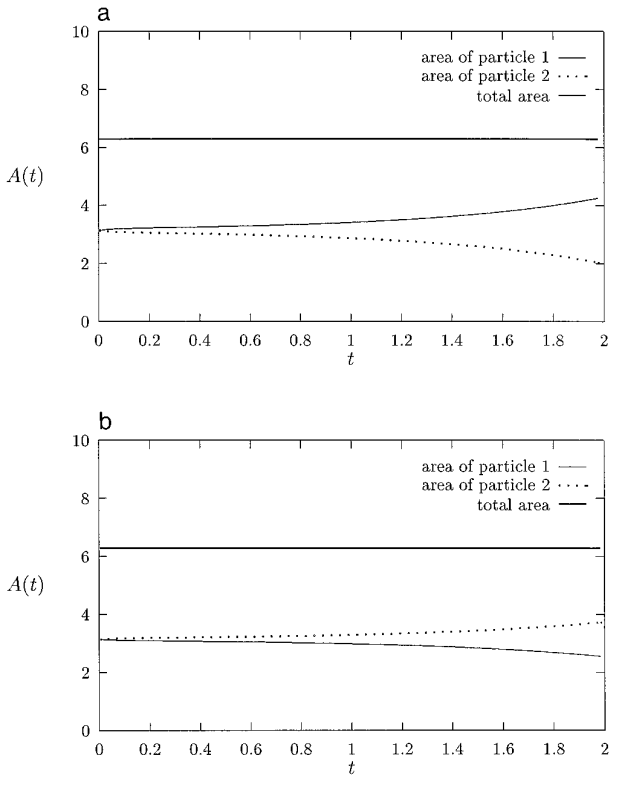

FIG. 8. Areas of the particles in two different configurations.

3. *if* $0 \le t < \tau < T$, *then* $C_1(\tau)$ *is completely contained in* $C_1(t)$, *and* $C_2(t)$ *is completely contained in* $C_2(\tau)$; *namely*, C_1 *is shrinking, whereas* C_2 *is expanding.*

Remark 4.1. Note that $a \sim d$. Hence, if $d(0) \gg R_2(0)$, then one can see that the terms we dropped from the original system (i.e., the terms starting with $n = 2$ in the expansion of $[u_n]$ in (4.2)) are of order $O((R_2/d)^2)$.

5. NUMERICAL RESULTS AND DISCUSSIONS

We begin our numerical calculations by studying the evolution of a single curve. It is believed that most simply-connected closed curves will circularize. First we look at the evolution of an ellipse with major axis 2 and minor axis 1. We place 256 points on the initial curve and use the equal arclength parametrization algorithm to reparametrize the curve. In Fig. 1a, we plot the curves at $t = 0$, 0.244, 0.494, and 0.994. Clearly the ellipse turns to a circle in a rather short time. We note that the initial motion is concentrated around the large curvature region. The early time steps are controlled by the large velocity there, and the CFL condition (3.3) is enforced; they are smaller than the largest time step allowed (0.0025) in the first seven steps ($t < 0.012$). This indicates that localized convex regions can be smoothed in a very short time.

To show some examples with less symmetry, we perturb the ellipse by

$$x(\alpha) = 1.5(1 + 0.1 \sin(2\alpha)) \cos(\alpha), \quad y(\alpha) = \sin(\alpha).$$

The result is shown in Fig. 1b. As we can see, the dynamics of this curve is very similar to the case in Fig. 1a. This shows that the circle is rather stable in this motion.

In Fig. 2 we look at a dumbbell shaped curve generated by the curvature distribution

$$\kappa(\alpha) = 1 + 2.3 \cos(2\alpha), \quad 0 \le \alpha \le 2\pi. \tag{5.7}$$

We use only 128 points here, since the initial curvature is represented by only two modes in the Fourier space. The largest time step allowed is 0.005. Due to the large curvature variation, the initial velocity is rather large, compared to the previous example. At $t = 0.043$, the curve is almost convex and turns to a track field object. Then it circularizes, and by the time $t = 0.15$, is almost circular.

Next, we study some multi-piece cases. To deal with the situation that some curve may be reduced to a point, we implement the following procedure: first, we will delete

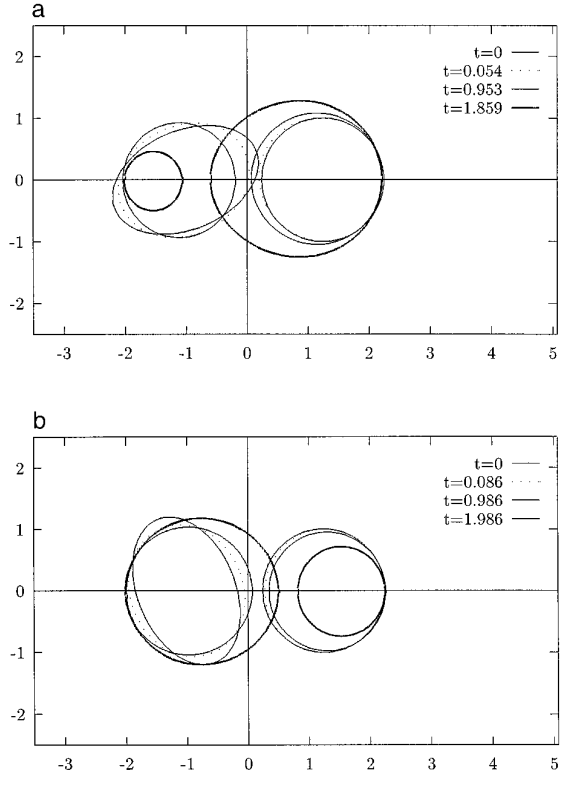

FIG. 9. Two particles with the same initial mass (area), but different shapes, $N = 256$: (a) the major axis of the initial ellipse has an angle of $\pi/8$ with x-axis; (b) the minor axis of the initial ellipse has an angle of $\pi/8$ with the x-axis.

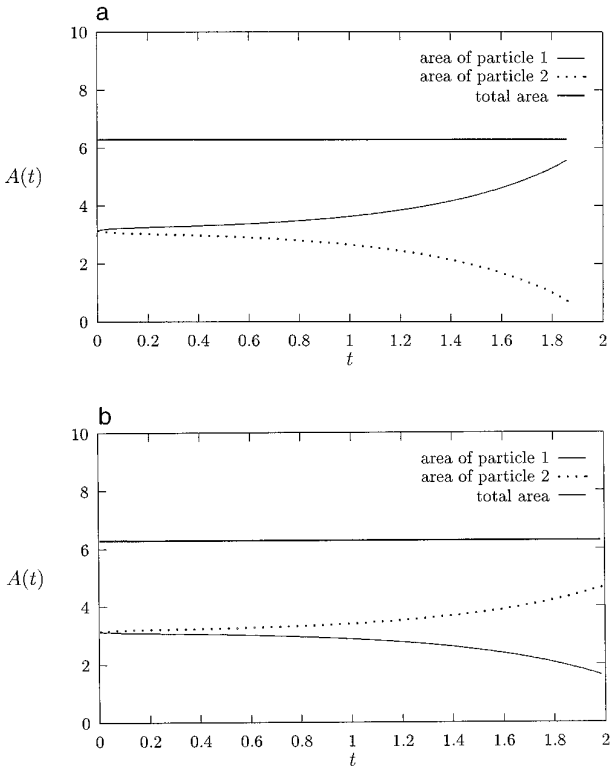

FIG. 10. Areas of the particles in two different configurations, with the initial ellipse rotated by an angle of $\pi/8$.

half of the points on a curve after the total arclength of the curve is reduced by a half, and the deleting process will continue every time the total arclength is halved; once there are only four points left on the curve, we assume that this curve can be ignored. We either stop the calculation or continue after deleting this particular curve. Similarly, points can be doubled once the arclength of a particular curve is doubled. It is necessary to delete or add points on some curves to maintain the regular distribution of points on different curves. This also helps with the requirement of the CFL condition (3.3).

To validate our method and test it for multiply-connected domains, we turn to the case of two concentric circles studied in Section 5.1. We pick the initial conditions $R_1 = 1.2$ and $R_2 = 2$ and start with 128 points for both circles. As we predict from the exact solution, both circles will shrink, until the inner circle shrinks to the origin. In Fourier space, there is only one mode in both circles so our numerical approach can take advantage of the situation. We compare our numerical result of $R_1(t)$ (which is equal to s_α^1) with the solution of (4.1), obtained by a numerical quadrature. In Fig. 3, we plot the solution as a function of t. According to the numerical quadrature, the inner circle will vanish around $t \approx 0.306869$ and our numerical calculation stopped around the same time. In the plot, we cannot distinguish between the two different functions. In fact, the l^2 norm of error is 8.6×10^{-4}. Another quantity of interest is the conserved area $A = \pi(R_2^2 - R_1^2)$. Our numerical solution gives a relative error about 0.01% in time consistently, except for the last 0.01 time unit where the relative error grows to 0.03%.

Our major interest in the applications of the method is to study the interaction of a large number of particles. We believe that with this efficient treatment, we can use a relatively small number of points for each particle to model a reasonably large particle system. In the following we present some examples; some of them will be comparable to the examples in [28].

We begin with two particles of different sizes. First we take two circles with radii 1 and 0.9, situated at (0, 0) and 2.1, 0), and start with 128 points for each curve. According to the results in [28], the larger particle will absorb the mass in the smaller one, and the smaller one will shrink to a point eventually. However, their calculations have to be halted at a certain time, as the time step can be so small due to the stability condition. Therefore, the interesting phenomenon of the smaller particle shrinking to a point was not observed. In our calculations, we do not have this

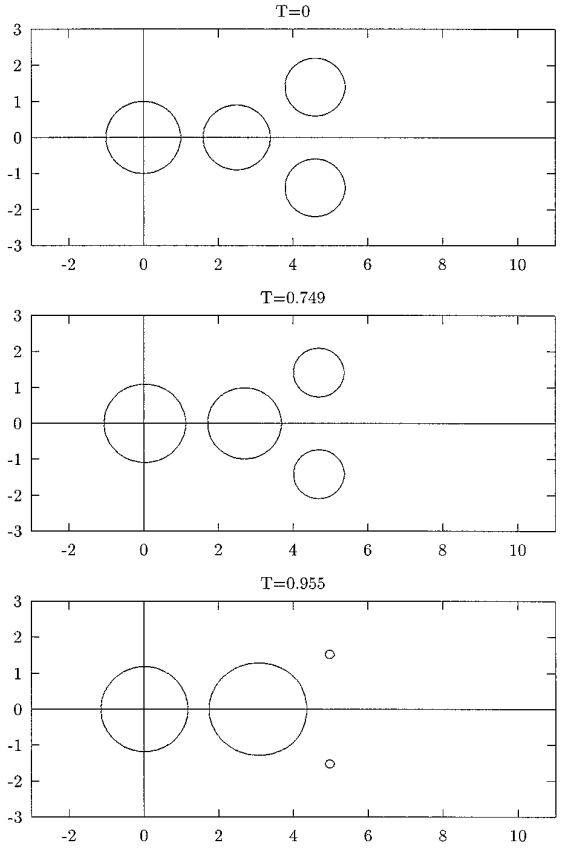

FIG. 11. A four-particle system, with two smaller particles initially situated near the particle in the center, $N = 512$.

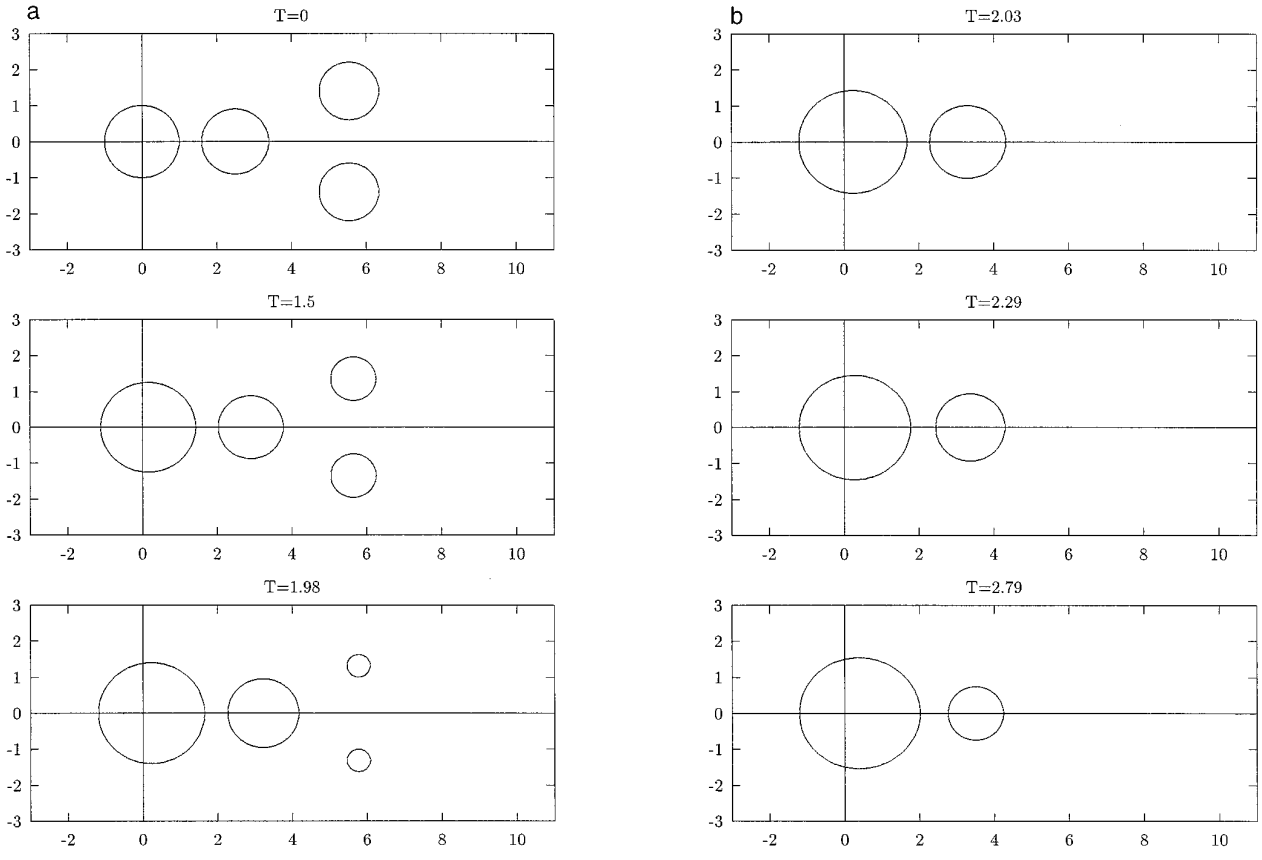

FIG. 12. A four-particle system, with two smaller particles initially shifted away from the particle in the center, $N = 512$: (a) early time before the smaller particles disappear; (b) later time after the smaller particles disappear.

problem. For this case, we continued until $t = 1.13$, when the smaller particle is so small that there are only four points left ($s_\alpha = 0.03536$ at this time). The solutions at different times are shown in Fig. 4a. Although in this example, the distance between the circles is not very large, and the two particles do not remain circular for $t > 0$, the conclusion of Lemma 4.1 seems to hold.

We remark that if we continue the calculation, then we have to start anew without the diminished particle. The subsequent motion becomes a single particle motion, and the curve will circularize, as shown in previous one-particle examples. We would like to mention, however, that the velocity field experiences a large jump at the moment we delete the ''tiny'' particle. In fact, the part of the large particle facing the right was moving towards the right when the smaller particle, no matter how small, was there; and the same part starts to move towards the left once the smaller particle is deleted, due to the circularizing effect. From a theoretical point of view, this is evident since a tiny circle has a large curvature, which contributes a large potential. Nevertheless, we expect, as shown in the exact solution for concentric circles, that the time it lasts is very short, and the total contribution is negligible. Of course, a detailed asymptotic analysis near the time of the topological changes would be extremely helpful. In fact, in a recent work by Chen [10], it is shown that, in the radially symmetric case, the subsequent motion of the asymptotic $\varepsilon \to 0$ limit of the Chan–Hilliard equation is obtained by simply removing the particle of zero radius. Since we know that the asymptotic limit of the Chan–Hilliard equation is the Mullins–Sekerka problem when the latter possesses a classical solution, it is reasonable to use the global time limit of the Cahn–Hilliard equation dynamics as the extension of motion of the Mullins–Sekerka problem beyond topological singularities. The analysis in [10] also indicates that as a general rule, when particles shrink to single points, the subsequent motion is obtained by removing these points. It should be pointed out that, in general, for other two-dimensional problems, removing a shrinking particle can have an $O(1)$ effect on the overall system, and special care should be taken when we deal with a particular physical model.

When two initially circular particles are far away from each other, the ODE system derived in Section 4.2 is expected to be a good approximation to describe the motion. We use the LSODE package to solve this ODE system

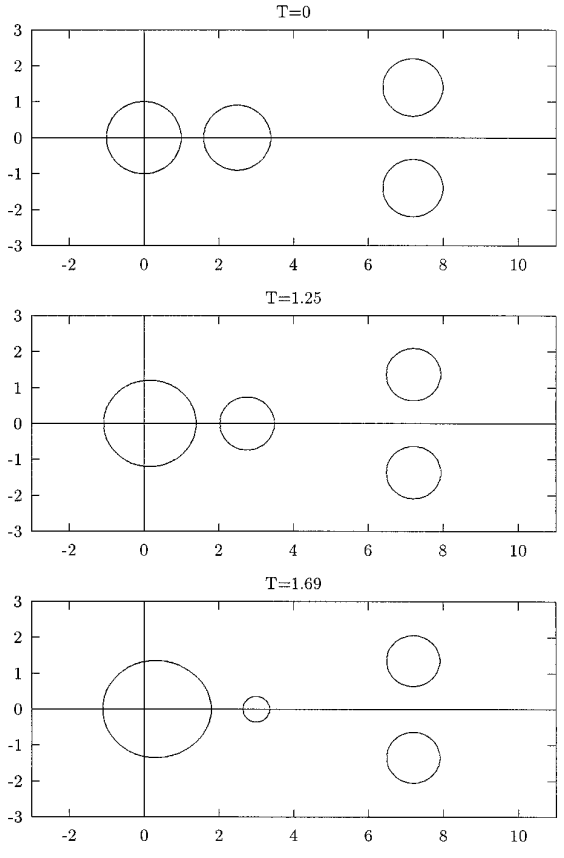

FIG. 13. A four-particle system, with two smaller particles initially shifted further away from the rest of the group, $N = 512$. The middle particle is about to disappear in the end of this calculation.

and compare it with the solutions of the exact equations using the method developed in this work. It turns out that the initial distance required to make the ODE system a reasonable approximation is not very large. This shows that the ODE system can be very useful to estimate interactions between two particles. In our example, we choose one circle of radius 0.9, situated at (4, 0), and another circle of radius 1, situated at (0, 0). Calculations are run from $t = 0$ to $t = 2$ in both the full free boundary problem and the simplified ODE problem. As we expect from the result in Lemma 4.1 and the previous example, the larger particle will absorb mass from the smaller particle, and both particles will shift to the right. The ODE system gives the evolutions of four parameters, namely, the radii and the centers of these two circles, by assuming the circular shape of particles. From our numerical calculations of the full equations, we obtain the areas, total arclengths, and centers of mass of these two particles. One measure to estimate the validity of the circular assumption for the ODE system is to check the value $A/(\pi s_\alpha^2)$ from the full equations, for each particle, where A is the area of the particle and s_α is the total arclength of the particle divided by 2π. In this example, this ratio is surprisingly close to one (the deviation from 1 is less than 10^{-4} most of the time). This shows that the circular assumption for particles is quite reasonable at this initial distance (the initial shortest distance between two circles is 2.1). As we compare the areas and centers of mass from two solutions, the difference turns out to be very small. In Fig. 5, we plot the difference as functions of t. Figure 5a shows the difference in areas, $A_i(t) - \pi R_i^2(t)$, $i = 1, 2$, where A_i is the area of particle i from the solution of the full equations, R_i is the radius of particle i from the solution of the ODE system. The fact that two curves for different particles are symmetric with respect to the t-axis shows that both solutions conserve the total area in time. Figure 5b shows the difference in centers of mass, $x_i^c - z_i$, where x_i^c is calculated from the solution of the full equations and z_i is calculated from the ODE system.

Next we consider the interaction of two initially noncircular particles, a case similar to the one studied in [28]. In Fig. 6b, we start with two ellipses: one is situated at $(-1, 0)$ with aspect ratio 0.5 and the other is situated at $(3, 0)$ with aspect ratio 2. We find that in the early stage, both ellipses circularize without much mass exchange. At $t = 0.3$, the smaller particle is almost circular and it starts to lose mass rapidly to the larger particle. This agrees with the finding in [28]. The difference we see is that the smaller particle sticks to the right edge of its initial shape, while in [28] the center of the smaller particle does not move so much towards the edge. This probably shows the two-phase

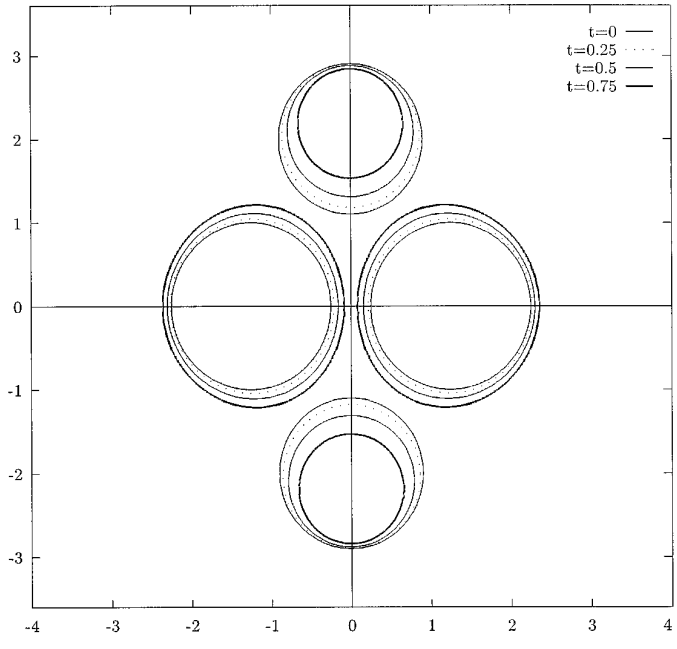

FIG. 14. Two pairs of particles with same areas and a symmetric configuration, $N = 512$. The larger pair is about to touch towards the end of this calculation.

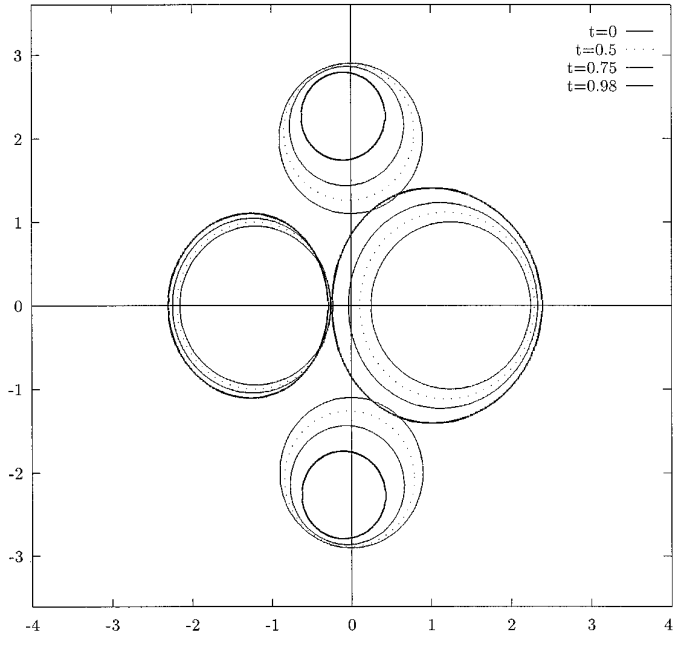

FIG. 15. Two pairs of particles with different areas, $N = 512$. The larger particles are about to touch towards the end of the calculation.

motion effect, compared to the one-phase calculations in [28].

It is natural to ask the question when we have two particles with the same mass (same area in this case): what is the effect of each particle in the interaction procedure? To understand this particular interaction mechanism, we perform a series of numerical experiments which consist of an initially circular particle and an initially elliptic particle, both with the same area π. In Fig. 7a, we start with a circle on the right, initially centered at (1.5, 0) and an ellipse with aspect ratio 25/16, initially centered at $(-1, 0)$. The ellipse circularizes very quickly and loses some mass during the circularization process. Then the same mechanism that appeared in Fig. 4 takes over. In Fig. 7b, we rotate the initial ellipse by an angle of $\pi/2$ and the opposite behavior happens. The areas of the particles and the total area of the system as functions of time are plotted in Fig. 8.

In Fig. 9, we rotate the ellipse and adjust the initial position of the circle (now at (1.25, 0)). First (in Fig. 9a) we see that the ellipse will be taken over by the circle when the major axis is more inclined towards the x-axis (the inclination angle is $\pi/8$). In Fig. 9b, when the major axis is more inclined towards the y-axis, the ellipse takes over. Particle area plots similar to Fig. 8 are given in Fig. 10. It is interesting to note that the mass transfer process is more rapid in the former case. This is probably due to the fact that the particles are closer in this case, where the ellipse is inclined.

When the inclination angle is $\pi/4$, it is suggested from the above behavior that it would be an unstable equilibrium. Our numerical result (not shown here) seems to support this speculation.

In the following, we study the effects of configuration for a collection of four initially circular particles and compare the results with that in [28]. All the calculations in this group start with 128 points for each particle. The basic configuration is shown in Fig. 11, where at $t = 0$ we have four circles with radii 1, 0.9, 0.8, and 0.8. The particles are numbered from the left to the right. The largest circle (particle 1) is situated at the origin, the second largest (particle 2) is situated at (2.5, 0), and the two smaller ones (particle 3 and 4) are situated at (4.6, $\pm$1.4). In this configuration, particle 2 has the advantage of being closer to the two smaller particles than particle 1. As a result, particle 2 grows at a faster rate than particle 1 and later surpasses particle 1 in size. At $t = 0.955$, the smaller particles have become very small ($s_\alpha = 0.1196$) and particle 2 has become the dominant particle in the group. It is noticed that the center of particle 2 has been shifted towards the right, corresponding to the fact that it has absorbed much of the mass in particle 3 and particle 4.

If we move these two smaller particles farther away from the larger particles, the interactions are weakened and the evolution process slows down a little. As we see in Fig. 12, where the initial centers for particle 3 and 4 are (5.55, $\pm$1.4), by the time $t = 1.5$, particles 3 and 4 have not lost much of their masses, compared with the previous case. During this time period, particles evolve rather slowly and

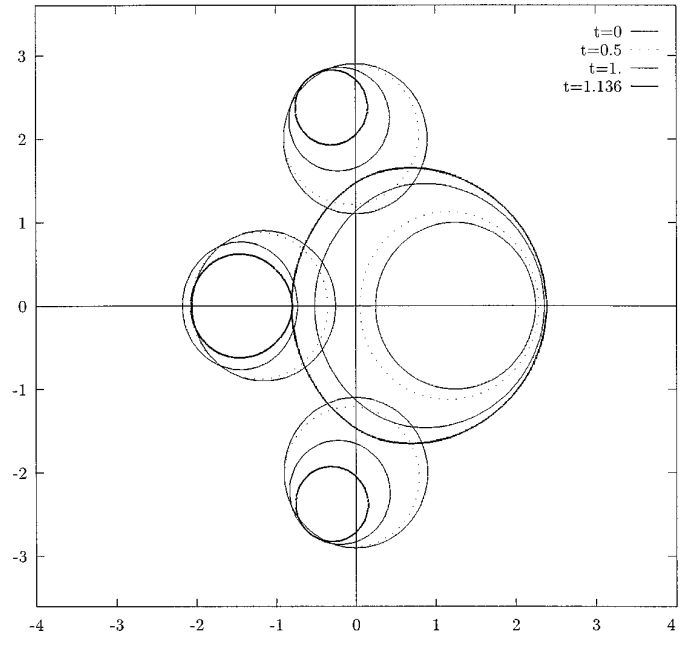

FIG. 16. One larger particle versus three smaller particles, $N = 512$, with the larger particle taking mass away from all three smaller particles.

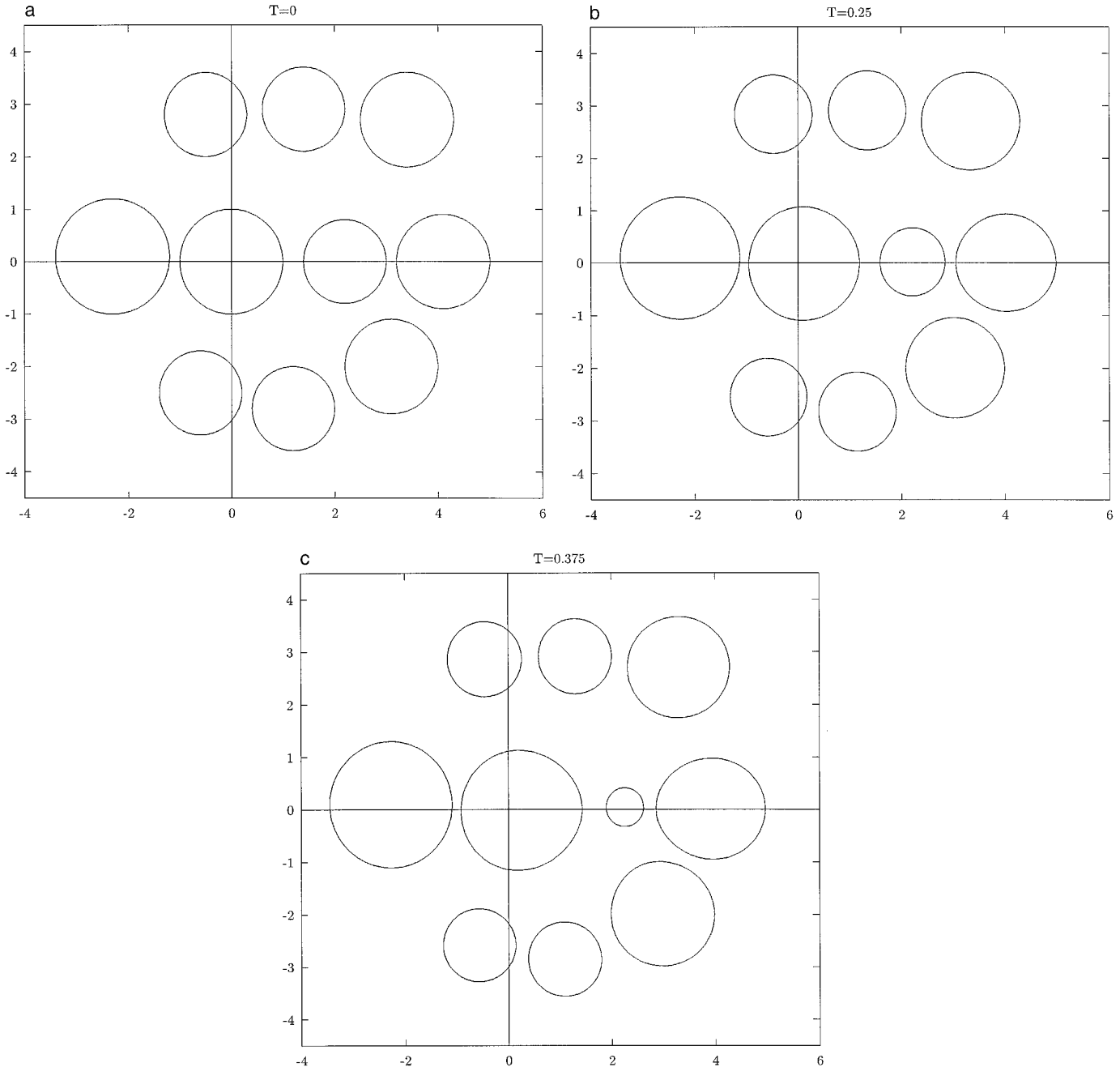

FIG. 17. A 10-particle system; total $N = 1280$: (a) $t = 0$; (b) $t = 0.25$; (c) $t = 0.375$; (d) $t = 0.404$; (e) $t = 0.615$, with only 9 particles left in the system.

particle 1 is still the dominant particle in the group. In the next stage, the evolution gains some momentum and by the time $t = 1.98$, the smaller particles have lost their masses substantially ($s_\alpha = 0.3158$). At $t = 2.03$, they become so small ($s_\alpha = 0.029$) that they are deleted. Similar to the results in [28], we also note a substantial migration distance of the center of mass of particle 2 during the process. Both particles 1 and 2 have absorbed the masses of particles 3 and 4, as we can check from the values of s_α of these two particles. Over the time period [0, 2.03], s_α for particle 1 increases from 1 to 1.436, and s_α for particle 2 decreases from 0.9 at $t = 0$, to 0.8743 at $t = 1.46$; then it increases to 1.0133 at $t = 2.03$. It is interesting to note the decreasing–increasing behavior of particle 2. One explanation is that as particle 2 migrates towards the smaller particles, it becomes easier for it to absorb the masses from particles 3 and 4. While initially it is quite close to particle 1 and far away from particles 3 and 4, so the main effect in the early time

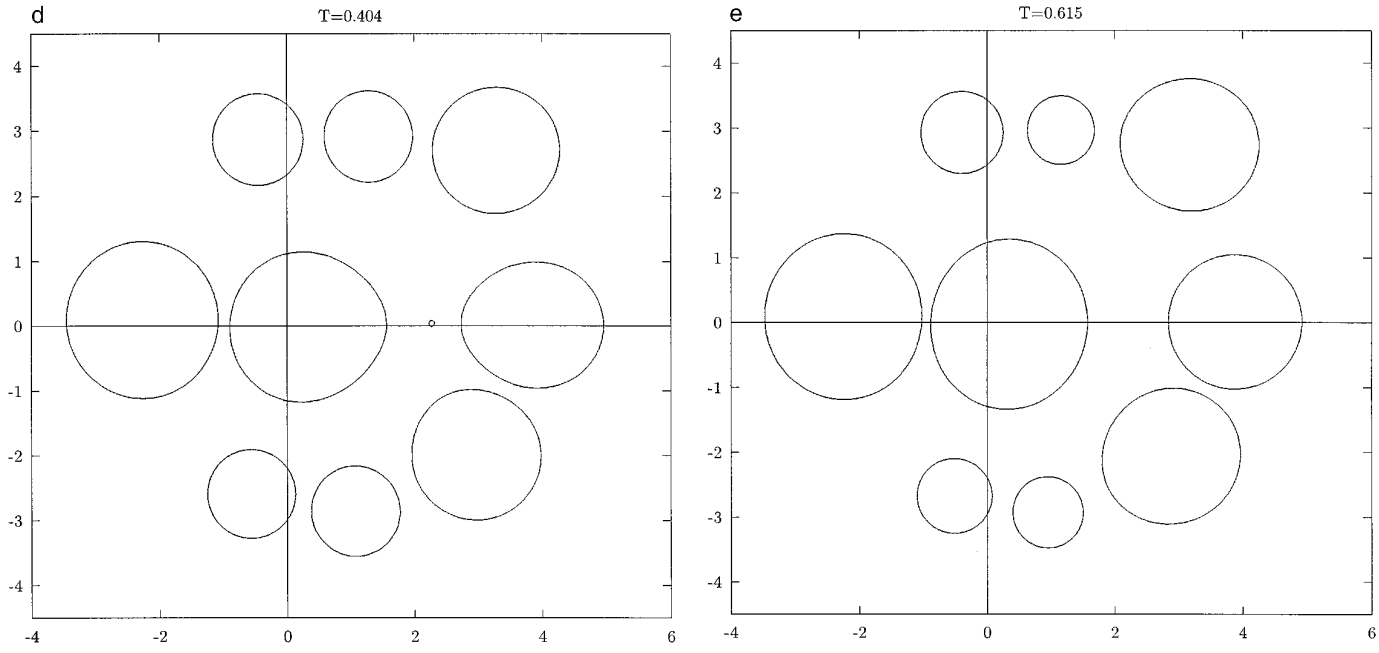

FIG. 17—*Continued*

is losing mass to particle 1. If we decide to continue the calculation, the result of the two-particle interaction will lead us to the situation where the dominant particle (particle 1) is going to eventually absorb all the mass in particle 2.

In Fig. 13, we push the initial positions of particles 3 and 4 to (7.2, ±1.4). In this case, we have two subgroups, relatively away from each other. Particles in the same group will interact with each other only, almost ignoring the presence of the other group. As a result, in group A, where particle 1 and particle 2 belong, the typical process as observed in Fig. 3 repeats itself here, with particle 1 taking over particle 2. However, the process is much slower now, compared to the two-particle interaction example in Fig. 3. In Fig. 3, the smaller particle disappears at $t = 0.955$, while here at $t = 1.69$ the smaller particle still has some mass ($s_\alpha = 0.366$). In group B (particles 3 and 4), since the two particles have the same size exactly, they would be in an equilibrium if there were no outside interaction. The presence of group A will take some masses away from this group, but at a rather low rate. To see this, we look at the s_α values in different times. Although these particles are no longer circular after $t = 0$, s_α values still serve as a good indicator to measure the particle size. In this case, the s_α values start with 0.8, at $t = 1.69$ they are still 0.71. They have not changed much during this time period.

In the above group of calculations, a singularity appears when some particle is confined to a very small area and some surgical efforts need to be made to continue the calculations. As mentioned earlier it would be very effective and sometimes necessary to know the asymptotic behavior of the shrinking process, especially the rate of s_α decreasing to zero. From the exact solution of the two concentric circles case, some knowledge of this behavior can be gathered. We hope this can be generalized to an arbitrary case and some approach combining the point source approximation with the boundary integral formulation would handle the small particles efficiently.

Another singularity that is more difficult to deal with both theoretically and numerically is the merging of several particles. We use an example similar to one found in [28] to study this problem. In Fig. 14, we start with four circles, each with 128 points. The two larger circles have the same radius 1, and they are situated at (±1.25, 0). The two smaller particles have the same radius 0.9, and they are situated at (0, ±2). As a consequence of the fact that the larger particles will grow, they will move closer to each other; eventually they will collide. At $t = 0.75$, the calculation has to be halted, due to the increasingly large velocities along the part of the curve where they are about to touch. The time scale here is much smaller than the regular time scale when particles are well separated.

In Fig. 15, we modify the configuration in Fig. 14, so the left particle has the initial radius 0.95, instead of 1. In this case, the calculation can be extended to $t = 0.984$. We see that the right particle crosses the center line (x-axis) and tends to touch the left particle.

As we further modify the configuration of this case by changing the radius of the left particle to 0.9 (Fig. 16), we

TABLE I

Particle	1	2	3	4	5	6	7	8	9	10
x-coord	0.	2.2	4.1	−0.6	1.2	3.1	−0.5	1.4	3.4	−2.3
y-coord	0.	0.	0.	−2.5	−2.8	−2.	2.8	2.9	2.7	0.1
Radius	1.	0.8	0.9	0.8	0.8	0.9	0.8	0.8	0.9	1.1

are able to run the calculation to 1.136. In the early times, it does not necessarily indicate that the right particle is going to touch the smaller particles. However, in the later times, this becomes more obvious. By $t = 1.136$, we see that the larger particle touches the left particle.

In our last example, we simulate a 10-particle system. They are randomly picked and distributed initially. Each particle has 128 points to start with. The positions and radii of these particles are listed in Table I.

As we see from Fig. 17, particle 2 is surrounded by four larger particles (1, 3, 6, and 9) and other particles of the same size. Obviously, it is the most vulnerable in the family. At $t = 0.25$, we do not find very appreciable changes in the family, except for this particle, which has lost quite a lot of its mass. At $t = 0.375$, particle 2 is even smaller, and particles 1 and 3 clearly have absorbed most of the mass in particle 2, as they become more and more non-circular, with expansion towards particle 2. By the time $t = 0.404$, particle 2 is almost gone, with particle 1 gaining so much from it that it is large enough to be able to compete with particle 10. If we are allowed to delete particle 2 after it has only four points left, we can continue our calculation to $t = 0.615$. At this time, particle 1 has become the dominant particle in the group and particle 10 has already lost mass to it. To show how effective these calculations are, we counted the CPU time for this particular run. Each time step takes about 15 CPU units on a SGI Indigo-2 R4400 workstation. There are 400 time steps in this calculation. The typical number of iterations it takes to solve the integral system in this calculation is about 50.

6. CONCLUSION

In this paper, we developed a very effective method to solve the Mullins–Sekerka free boundary problem. The $\theta - L$ formulation allows us to solve the evolution equations implicitly, in the Fourier space, so solutions can be obtained for a very long time and interesting dynamic behaviors are observed. This method can adjust adaptively the number of points needed to describe a particle and can delete a particle automatically when it is small enough. Using this method, we have successfully studied many systems with either one particle or many particles. Our numerical results confirm that a single, but not too complicated drop tends to circularize. In two-particle systems, the mass transfer process will let one particle eat up the other one. In particle systems with more than two particles, the competition is complicated. A particle grows or shrinks, depending not only on its relative size to the others, but also on the surrounding particle configurations.

What remains to be answered is the question of what happens when topological singularity arises. With some reconnecting mechanism, our method can be modified to include this complicated phenomenon. For example, when two different points of a particle become very close to each other, this single particle can be broken into two separated pieces. Similarly, if two points from different particles get very close, these two particles can be connected to become one particle. We believe that our method can be further developed for some other physical laws concerning the topological changes when singularities occur. We hope that in our future research, we can answer these questions both theoretically (such as a continuation study of [10]) and numerically. For systems of a large number of particles, we note that the fast multipole algorithm [17] can be used in our formulation to speed up the evaluation of the integrals. However, with a large number of particles, some particles are bound to collide in a finite time. This suggests that the reconnection issue has to be resolved before any meaningful calculations for a large number of particles can be performed. It should be pointed out that this single layer formulation cannot be extended to solve the nonsymmetric solidification problem, where the jump condition for the normal derivative of the temperature is replaced by a more general flux condition involving different coefficients on different sides of the interface. It is a much more realistic model and, in this case, adding a double layer presumably would solve the problem. Currently we are studying the possibility of extending the approach presented here to a double-layer formulation.

ACKNOWLEDGMENTS

X. C. is thankful for the financial support of the Alfred P. Sloan Research Fellowship and the National Science Foundation Grant DMS-9404773. T. Y. H. is thankful for the financial support of the National Science Foundation Grant DMS-9407030 and the Department of Energy Grant DE-FGO3-89ER25073. The calculations were performed at the Center for Scientific Computing at the University of Utah.

REFERENCES

1. N. D. Alikakos, P. W. Bates, and X. Chen, *Arch. Rat. Mech. Anal.,* **128,** 165 (1994).
2. Akaiwa and D. Meiron, *Phys. Rev. E,* submitted for publication.
3. G. Baker, D. Meiron, and S. Orszag, *J. Fluid Mech.* **123,** 477 (1982).
4. G. Baker, in *Waves in Fluids,* edited by R. E. Meyer, p. 53 (Academic Press, New York, 1983).
5. G. Baker and M. J. Shelley, *J. Comput. Phys.* **64,** 112 (1986).

6. P. Bates, X. Chen, and X. Deng, *Electro. J. Differ. Eqn.* 1995, No. 11, 1 (1995).
7. J. F. Blowey and C. M. Elliott, "A Phase Field Model with Double Obstacle Potential," in *Motion by Mean Curvature and Related Topics,* edited by G. Buttazzo and A. Visintin, p. 1 (de Gruyter, New York, 1994).
8. G. Caginalp and X. Chen, *Eur. J. Appl. Math.,* to appear.
9. J. W. Cahn and J. E. Hilliard, *J. Chem. Phys.* **28,** 258 (1958).
10. X. Chen, *J. Differ. Geom.,* to appear.
11. X. Chen, *Arch. Rat. Mech. Anal.* **123,** 117 (1993).
12. X. Chen, X. Hong, and F. Yi, preprint.
13. W. Dai and M. J. Shelley, *Phys. Fluids A* **5,** 2131 (1993).
14. A. J. DeGregoria and L. W. Schwartz, *J. Fluid Mech.* **164,** 383 (1986).
15. J. Duchon and R. Robert, *Ann. Inst. H. Poincaré Anal. Non Linéaire* **1,** 361 (1984).
16. A. Greenbaum, L. Greengard, and G. B. McFadden, *J. Comput. Phys.* **105,** 267 (1993).
17. L. Greengard and V. Rokhlin, *J. Comput. Phys.* **73,** 325 (1987).
18. T. Y. Hou, J. S. Lowengrub, and M. J. Shelley, *J. Comput. Phys.* **114,** 312 (1994).
19. H.-J. Jou, P. H. Leo, and J. S. Lowengrub, University of Minnesota Supercomputer Institute Research Report UMSI 95/177.
20. D. A. Kessler, J. Koplik, and H. Levine, *Phys. Rev. A* **30,** 3161 (1984).
21. R. Krasny, *J. Fluid Mech.* **167,** 65 (1986).
22. W. W. Mullins and J. Sekerka, *J. Appl. Math.* **34** (1963), 322–329.
23. R. L. Pego, *Proc. R. Soc. London Ser. A* **422,** 261 (1989).
24. J. A. Sethian and J. Strain, *J. Comput. Phys.* **98,** 231 (1992).
25. M. J. Shelley, *J. Fluid Mech.* **244,** 493 (1992).
26. J. Strain, *J. Comput. Phys.* **85,** 342 (1989).
27. G. Tryggvason and H. Aref, *J. Fluid Mech.* **136,** 1 (1983).
28. P. W. Voorhees, G. B. McFadden, Boisvert, and D. I. Meiron, *Acta Metall.* **36,** 207 (1988).